Monatshefte für Chemie 133, 1497–1534 (2002)
DOI 10.1007/s00706-002-0502-y

Monatshefte für Chemie
Chemical Monthly
Printed in Austria

Invited Review

Multiple-Quantum Magic-Angle Spinning: High-Resolution Solid State NMR Spectroscopy of Half-Integer Quadrupolar Nuclei

Amir Goldbourt[1] and **Perunthiruthy K. Madhu**[2,*]

[1] Department of Chemical Physics, Weizmann Institute of Science, Rehovot 76100, Israel
[2] Department of Chemistry, University of Southampton, Southampton SO17 1BJ, United Kingdom

Received April 16, 2002; accepted May 6, 2002
Published online September 19, 2002

Summary. Experimental and theoretical aspects of the multiple-quantum magic-angle spinning experiment (MQMAS) are discussed in this review. The significance of this experiment, introduced by *Frydman* and *Harwood*, is in its ability to provide high-resolution NMR spectra of half-integer quadrupolar nuclei ($I \geq 3/2$). This technique has proved to be useful in various systems ranging from inorganic materials to biological samples. This review addresses the development of various pulse schemes aimed at improving the signal-to-noise ratio and anisotropic lineshapes. Representative spectra are shown to underscore the importance and applications of the MQMAS experiment.

Keywords. NMR spectroscopy; Solid state; Quadrupolar nuclei; MQMAS; Amplitude modulation.

Introduction

The internal spin interactions in solid state nuclear magnetic resonance (NMR) that chiefly govern the spectral response are quadrupolar (Q), dipole–dipole (DD), chemical shift anisotropy (CSA), and scalar coupling (J). These interactions are in general anisotropic in character. The quadrupolar interaction vanishes in the case of spin-$\frac{1}{2}$ nuclei like ^{1}H and ^{13}C due to the internal spherical symmetry of the nuclear spin system. This is not the case for nuclei with spin quantum number $I \geq 1$. These nuclei possess an electric quadrupolar moment (also called nuclear quadrupole moment) in addition to having a nuclear magnetic moment as in the case of spin-$\frac{1}{2}$ nuclei. This nuclear quadrupole moment couples to the inhomogeneous

* Corresponding author. E-mail: madhu@soton.ac.uk

internal electric field gradients (EFG) [1]. The interaction of the nuclear quadrupole moment with a non-vanishing EFG at the nuclear site leads to a modification of the *Zeeman* energy levels and dominates the appearance of an NMR spectrum. The nature of EFG depends on the local electronic environment and symmetry about the nucleus. Hence, if the characteristics of the EFG can be determined from NMR experiments, information about the chemistry of a molecule, and details about the molecular or the crystalline environment can be ascertained.

Quadrupolar nuclei can be classified into those with integer spins (1, 3, etc.) and half-integer spins ($\frac{3}{2}, \frac{5}{2}$, etc.). Some prominent nuclei that fall into the class of spin-1 are deuterium (^{2}H) and nitrogen (^{14}N), spin-3 is boron (^{10}B), spin-$\frac{3}{2}$ are sodium (^{23}Na), rubidium (^{87}Rb), and boron (^{11}B), spin-$\frac{5}{2}$ are oxygen (^{17}O), aluminium (^{27}Al), and molybdenum (^{95}Mo), spin-$\frac{7}{2}$ are cobalt (^{59}Co), calcium (^{43}Ca), and scandium (^{45}Sc), and spin-$\frac{9}{2}$ is niobium (^{93}Nb). A survey of the periodic table shows that around 70% of the elements are quadrupolar in nature.

Several techniques are available to obtain a high-resolution spectrum of spin-$\frac{1}{2}$ nuclei by decoupling experiments and systematically probing the anisotropy of the interactions by recoupling experiments [2]. However, in samples containing quadrupolar nuclei, unless there is a spherical charge distribution around the nucleus, which occurs only in a few cases, the quadrupolar interaction far exceeds DD, CSA, and J interactions. Typically, the quadrupolar interactions vary from a few kHz to a few MHz leading up to 2000–3000 MHz in the case of ^{127}I.

Due to their abundance, quadrupolar nuclei are dominant in several molecular systems ranging from porous materials, ceramics and glasses, to superconductors and biological systems such as nucleic acids and proteins. The practical applications of quadrupolar nuclei in several branches of science were discussed a long time ago by *Pound* [3]. Two factors have impeded the routine study of these materials. One is the line broadening in a powder sample arising from the size of the quadrupole moment that causes lack of resolution in currently available spectrometers and secondly, the complexity in spin dynamics due to the presence of more than two energy levels. This renders development of pulse methodology a demanding task as against the scenario in spin-$\frac{1}{2}$. Utilising the established spin-$\frac{1}{2}$ techniques does not always provide the required result. For example, magic-angle-spinning (MAS) [4, 5] does not provide isotropic high-resolution spectra in quadrupolar systems and cross-polarisation (CP) to and from such nuclei are normally not efficient [6, 7]. Hence, although rich in information content (e.g. in ^{2}H systems), and sometimes enabling an easier interpretation of the spectrum, high-resolution quadrupolar split spectra in the solid state are difficult to acquire with conventional spin-$\frac{1}{2}$ means.

In order to overcome the resolution problems in quadrupolar systems, mechanical ways were first devised. This resulted in two ingenious attempts, namely, double rotation, DOR [8] and dynamic angle spinning, DAS [9, 10], both involving manipulation of the spatial part of the quadrupolar Hamiltonian. Recent attempts focussed on the manipulation of the spin part of the Hamiltonian and this paved the way to the introduction of MQMAS [11, 12] by *Frydman* and *Harwood*, and lately, satellite transition MAS (STMAS) by *Gan* [13]. The introduction of MQMAS led to a spurt of activities that saw a large number of applications and improvements of this scheme. The popularity of this technique as against its forerunners can be understood from the simplicity of the experimental protocol with no need for

any extra hardware and demanding spectrometer performance efficiency. Development in this area has also shed more light on the complicated spin dynamics of quadrupolar nuclei.

In this review, we deal mainly with MQMAS, and refer to [14–16] for details on DOR, DAS, and STMAS. Many of the basic properties of the quadrupolar Hamiltonian have been dealt with in a succinct manner by *Vega* [17] and we borrow on them extensively here giving the appropriate equations wherever necessary.

The outline of this review is as follows: Introduction to the quadrupolar Hamiltonian under MAS, the technique of MQMAS and interpretation of MQMAS spectra, possible solutions to the problem of sensitivity, some heteronuclear techniques, and finally a few representative applications and future perspectives.

Quadrupolar Spins – Theory and Methods

The quadrupolar Hamiltonian, $\mathcal{H}_Q$, besides being stronger than the other internal spin Hamiltonians, is often stronger than typical radiofrequency (rf) fields employed in NMR. For an analysis of quadrupolar spectra, the first two terms in the expansion of $\mathcal{H}_Q$ are considered: the first-order, $\mathcal{H}_Q^{(1)}$, and second-order, $\mathcal{H}_Q^{(2)}$, following standard perturbation theory.

Figure 1 shows the energy levels of spins $I = \frac{3}{2}$ and 1 in a *Zeeman* field ν_0 in the absence and presence of a quadrupolar interaction ν_Q. Also shown is a schematic of the resultant quadrupolar split NMR spectra for the case of a single crystal. The quadrupolar interaction shifts the eigenvalues of the *Zeeman* Hamiltonian, resulting in an NMR spectrum that is split into $2I$ peaks. In a powdered sample, lines are broadened by the orientation dependence of the first- and second-order quadrupolar interactions.

The first-order quadrupolar interaction affects only the satellite transitions $m \leftrightarrow m \pm 1$, where $|m|$ takes the values $\frac{1}{2}, \frac{3}{2}, \frac{5}{2}, \cdots$. Thus, in the case of integer spins, the observable satellite transitions are broadened extensively (up to several MHz), making their detection cumbersome (an exception is deuterium, ^{2}H, which possesses a relatively small quadrupolar coupling constant (≈ 200 kHz), hence being a commonly probed nucleus). The broadening is a result of the significant shift the energy levels experience due to $\mathcal{H}_Q^{(1)}$. However, the symmetric transitions $m \leftrightarrow -m$ are affected only by the relatively smaller second-order quadrupolar interaction. Hence, the observable single-quantum transition of half-integer quadrupolar spins, $-\frac{1}{2} \leftrightarrow \frac{1}{2}$, is broadened only by $\mathcal{H}_Q^{(2)}$. This transition, called the central transition, thus provides a relatively narrow powder lineshape, which retains all information about the nuclear quadrupole coupling constant, NQCC, and the asymmetry of the quadrupolar interaction tensor, η.

NQCC characterises the size of the quadrupolar interaction experienced by a particular nucleus and is given in frequency units by e^2qQ/h, denoted by χ. Here, eq is the magnitude of the EFG and eQ is the nuclear electric quadrupole moment in units of the electronic charge e [18]. The quadrupolar frequency ν_Q in units of Hz or ω_Q in units of rad s^{-1}, is given by [1],

$$\nu_Q = \frac{\omega_Q}{2\pi} = \frac{3\chi}{2I(2I-1)}. \tag{1}$$

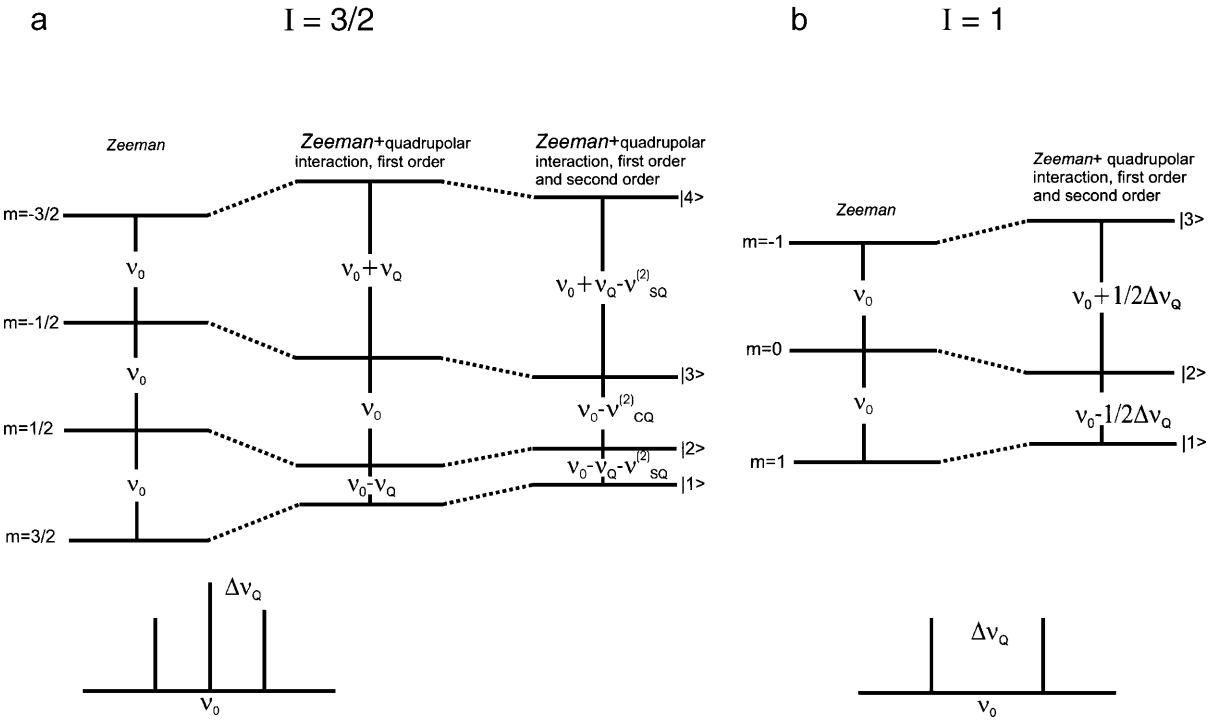

Fig. 1. Energy levels of a spin-$\frac{3}{2}$ and a spin-1 quadrupolar system in the presence of *Zeeman* field, first-order quadrupolar and second-order quadrupolar interactions. The allowed transitions, $\Delta m = \pm 1$, are indicated. The stick spectra at the bottom are the quadrupolar split spectra for a single crystal. ν_Q is the first-order quadrupolar frequency, $\nu_{CQ}^{(2)}$ and $\nu_{SQ}^{(2)}$ are the second-order quadrupolar frequencies of central and satellite transitions respectively, $\omega_0 = 2\pi\nu_0$ is the *Larmor* frequency, and $\Delta\omega_Q = 2\pi\Delta\nu_Q$ is the quadrupolar splitting

Hence, for a spin-$\frac{3}{2}$, for example, $\nu_Q = \frac{1}{2}\chi$, and for a spin-$\frac{5}{2}$, $\nu_Q = \frac{3}{20}\chi$. The NQCC vanishes for those quadrupolar nuclei positioned at a cubic site due to the inherent symmetry. The second-order quadrupolar interactions scale as $\frac{\nu_Q^2}{\nu_0}$. Hence, a higher resolution is obtained at higher magnetic fields for the same quadrupolar strength.

The MAS Hamiltonian

The general form of the quadrupolar Hamiltonian in the notation of irreducible tensor operators [1, 17] is given in Eq. (2) as

$$\mathcal{H} = \frac{\nu_Q}{3}\sum_{k=-2}^{2}(-1)^k T_q^{(2)} V_{-q}^{(2)} \tag{2}$$

with

$$\begin{aligned} T_0^{(2)} &= \sqrt{\frac{1}{6}}[3I_z^2 - I(I+1)] \\ T_{\pm 1}^{(2)} &= I_z I_\pm = I_\pm I_z \\ T_{\pm 2}^{(2)} &= I_\pm^2 . \end{aligned} \tag{3}$$

The elements $V_q^{(2)}$ are obtained from the components of the quadrupolar tensor $\rho_m^{(2)}$ in their principal axis system (PAS) by a transformation to the laboratory frame using the *Euler* angles α, β, γ:

$$V_q^{(k)} = \sum_{q'=-k}^{k} \rho_{q'}^{(2)} D_{q'q}^{(2)}(\alpha, \beta, \gamma). \tag{4}$$

The terms $D_{q'q}^{(k)}(\alpha, \beta, \gamma)$ are the *Wigner* matrix elements [19], and

$$\begin{aligned} \rho_0^{(2)} &= \sqrt{\frac{3}{2}} \\ \rho_{\pm 1}^{(2)} &= 0 \\ \rho_{\pm 2}^{(2)} &= -\frac{1}{2}\eta. \end{aligned} \tag{5}$$

In the laboratory frame the quadrupolar interaction can be treated as a perturbation to the *Zeeman* field, and can be expressed as a sum of first-order and second-order terms, as follows:

$$\begin{aligned} \mathcal{H}_Q &= H_Q^{(1)} + H_Q^{(2)} \\ H_Q^{(1)} &= \frac{\nu_Q}{3} T_0^{(2)} V_0^{(2)} = \frac{h\nu_Q'}{6}[3I_z^2 - I(I+1)] \\ H_Q^{(2)} &= \frac{h\nu_Q^2}{9\nu_0}\left\{ 2I_z\left[2I_z^2 - I(I+1) + \frac{1}{4}\right] V_{-1}^{(2)} V_1^{(2)} \right. \\ &\qquad \left. + I_z\left[I_z^2 - I(I+1) + \frac{1}{2}\right] V_{-2}^{(2)} V_2^{(2)} \right\} \end{aligned} \tag{6}$$

where ν_Q' is given by

$$\nu_Q' = \nu_Q\left(\frac{3\cos^2\beta - 1}{2} + \frac{\eta}{2}\sin^2\beta\cos 2\alpha\right). \tag{7}$$

Under MAS conditions, the PAS of the quadrupolar spin has to be first transformed into the rotor frame with the proper *Wigner* matrix $D(\alpha, \beta, \gamma)$. The angles (α, β, γ) describe the location of the rotor axis in the PAS of the quadrupolar tensor. Only then the transformation into the LAB frame is performed using $D(\omega_r t, \theta_{MA}, 0)$, $\omega_r t$ being the phase angle experienced by the rotor while spinning at the magic angle, θ_{MA} (54.7°) with respect to the static magnetic field. Thus Eq. (6) describes the MAS average Hamiltonian for the quadrupolar nucleus with a new definition of the terms $V_q^{(2)}$:

$$V_q^{(2)} = \sum_{m=-2}^{2} D_{mq}^{(2)}(\omega_r t, \theta_{MA}, 0) \sum_{n=-2}^{2} D_{nm}^{(2)}(\alpha, \beta, \gamma)\rho_n^{(2)}. \tag{8}$$

The terms $V_q^{(2)} V_{-q}^{(2)}$ in Eq. (6) contain products of *Wigner* matrix elements. These may be expanded using the *Clebsch-Gordon* coefficients [19]. Hence, in the fast spinning limit, the spatial part of the quadrupolar second-order Hamiltonian becomes a sum of *Legendre* polynomials with ranks 0, 2, and 4 (the terms with

ranks 1 and 3 vanish due to symmetry). After such an expansion, a straightforward calculation gives a simple expression for the symmetric transitions,

$$\nu_{m,-m} = \sum_{l=0,2,4} \nu_Q^{(l)}(\alpha,\beta,\gamma) C_l(I,m) P_l(\cos\theta_{MA}). \tag{9}$$

In Eq. (9) $P_l(\cos\theta)$ is the *Legendre* polynomial of rank l, and $C_l(I,m)$ are zero-, second- and fourth-rank (spin) coefficients depending on the spin quantum number I and order $2m$ of the transition. Their explicit forms may be found in Ref. [11] and are reproduced here:

$$\begin{aligned} C_0(I,m) &= 2m[I(I+1) - 3m^2] \\ C_2(I,m) &= 2m[8I(I+1) - 12m^2 - 3] \\ C_4(I,m) &= 2m[18I(I+1) - 34m^2 - 5]. \end{aligned} \tag{10}$$

Equation (9) is the basis of the MQMAS experiment as will be discussed later on. Additional details about the functional forms of lineshapes and shifts of quadrupolar nuclei can be found in Ref. [20, 21].

Magic-Angle Spinning Spectra

As outlined above, the central transition of non-integer quadrupolar spins is not affected by the first-order quadrupolar interaction. Hence, it is amenable to NMR spectroscopy using standard NMR techniques. Nevertheless, the existence of several energy levels complicates the excitation profile of a quadrupolar spin. While for a spin-$\frac{1}{2}$ system the nutation frequency ν_{nut} equals the rf field strength $\nu_1(=\gamma B_1)$, for a quadrupolar spin I, $\nu_{nut} = \left(I+\frac{1}{2}\right)\nu_1$. This equation holds goods as long as the excitation is selective, that is $\nu_1 \ll \nu_Q$. A hard-pulse excitation ($\nu_1 \gg \nu_Q$) gives a nutation frequency that is similar to a spin-$\frac{1}{2}$, $\nu_{nut} = \nu_1$. In the intermediate regime, a complex behaviour is expected and the nutation frequency of the central transition depends on ν_Q. Thus, in order to obtain a quantitative MAS spectrum, a small angle pulse $\left(\nu_1 t \leq \frac{\pi}{6}\right)$ has to be used [22, 23]. This ensures that in a sample of multiple sites with varying values of ν_Q, each site is uniformally excited. Figure 2 illustrates this aspect for a spin-$\frac{3}{2}$ nucleus.

Theoretical second-order quadrupolar broadened line shapes are given in Fig. 3 for both static and MAS cases for a few values of η. Although MAS achieves considerable line narrowing of the central transition (3 to 4 times with respect to the line width in a static case) it is still beyond what can be called a high-resolution quadrupolar spectrum.

The reason why MAS cannot narrow the second-order broadening can be seen directly from Eq. (9). The isotropic quadrupolar shift ($l=0$) is given explicitly in Eq. (11) as

$$\nu_{iso}^{(2)} = \frac{1}{30}\frac{\nu_Q^2}{\nu_0}\left[I(I+1) - \frac{3}{4}\right]\left(1 + \frac{1}{3}\eta^2\right). \tag{11}$$

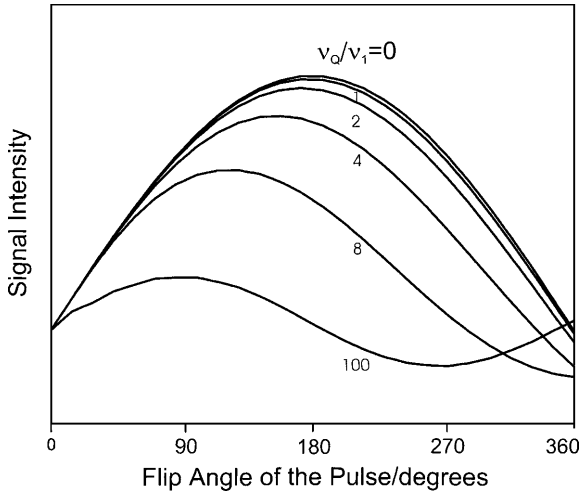

Fig. 2. The single-quantum signal intensity (normal MAS spectral intensity with a single pulse for excitation) plotted in arbitrary units as a function of the flip angle of the excitation pulse. The curves are calculated for different values of the ratio of the ^{23}Na quadrupolar frequency, ν_Q, to the rf field strength, $\nu_1 = 100.0$ kHz, as indicated against each curve. The MAS rate was 10.0 kHz and the ^{23}Na *Larmor* frequency was 91.25 MHz at a magnetic field of 8.1 T. This figure illustrates that the excitation of a powder sample is non-uniform, unless a small flip angle pulse is used

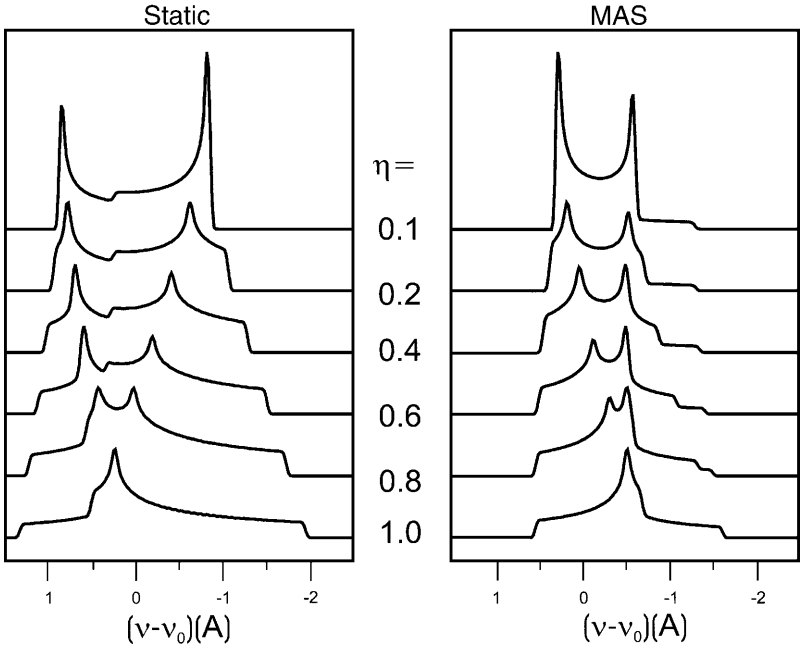

Fig. 3. Simulated second-order quadrupolar broadened central transition lineshapes of half-integer quadrupolar spins for both static and MAS conditions. The frequency scale is in units of A, given by $A = \frac{1}{9}\left[I(I+1) - \frac{3}{4}\right]\frac{\nu_Q^2}{\nu_0}$. Note that A is a universal parameter and, hence, the lineshapes do not depend on I, but the widths do

The product of the orientation dependent terms in Eq. (9) with the second- and fourth-rank *Legendre* polynomials, given in Eq. (12),

$$P_2(\cos\theta) = \frac{1}{2}(3\cos^2\theta - 1)$$
$$P_4(\cos\theta) = \frac{1}{8}(35\cos^4\theta - 30\cos^2\theta + 3) \qquad (12)$$

is the source for the line broadening of the central transition spectra, where θ is the angle of rotation axis with respect to the static external magnetic filed. It is evident from these equations that there are no common roots for both of them. Hence, a rotor spinning at the magic-angle, $\theta_{MA} = arc\tan 1/\sqrt{2}$, will zero the $P_2(\cos\theta)$ terms, but will always leave behind an anisotropic contribution from the $P_4(\cos\theta)$ terms that have roots at 30.56° and 70.12°. This anisotropic contribution gives rise to the partial broadening of the MAS lineshapes as depicted in Fig. 3.

While only the nutation behaviour of the central transition was discussed above, it should be noted that other transitions are also possible with $\Delta m = \pm 1$ (satellite transitions) and more importantly, those with $\Delta m = \pm 3, \pm 5, \ldots$ *i.e.* the symmetric transitions. The excitation of the multiple quantum symmetric transitions scales as $\nu_{MQ} \propto \frac{\nu_1^M}{\nu_Q^{M-1}}$, where M is the order of the excited coherence [24]. The possibility to directly excite these multiple-quantum transitions directly is also crucial for the success of the MQMAS experiment.

Resolution Enhancement Schemes

Before introducing MQMAS, we outline here a few experiments, all aimed to probe quadrupolar systems to obtain the relevant quadrupolar parameters. In addition to MAS, these include nutation spectroscopy [25], variable angle spinning (VAS) [26], and satellite transition spectroscopy [27]. Nutation spectroscopy and VAS allow determination of ν_Q and η from the second-order quadrupolar line shape of the central transition. Their applicability is limited to instances where the second-order quadrupolar line shapes can be readily resolved. Satellite transition spectroscopy gives quadrupolar parameters by a simulation of the complete manifold of spinning sidebands for the satellite transitions in the MAS NMR spectra of quadrupolar nuclei. This is possible, since, the broadening of the sidebands of the satellite transitions is smaller than those of the central transition. However, the manifold of sidebands extends over several MHz and a very accurate setting of the magic-angle is required. Yet, none of these methods achieves real high-resolution spectra since an inhomogeneous contribution to the quadrupolar interaction still remains.

The two experimental approaches that yielded ''real'' high-resolution spectra for the first time were double rotation (DOR) [8] and dynamic angle spinning (DAS) [9, 10]. DOR involves two rotors, an outer rotor, inclined at an angle of θ_1 with respect to the external magnetic field, and an inner rotor containing the sample having an axis of rotation that makes an angle of θ_2 with the outer rotor. The DOR condition can be stated as, Eq. (13),

$$P_2(\cos\theta_1)P_2(\cos\theta_2) = 0$$
$$P_4(\cos\theta_1)P_4(\cos\theta_2) = 0, \qquad (13)$$

with their solutions, Eq. (14), being either

$$\{\theta_1, \theta_2\} = \{54.73^\circ, 30.56^\circ\} \quad \text{or}$$
$$\{\theta_1, \theta_2\} = \{54.73^\circ, 70.12^\circ\}. \tag{14}$$

The DAS scheme makes use of only one rotor, but the orientation of the rotor axis with respect to the external magnetic field toggles between two angles for two equal periods of time. It is a two-dimensional (2D) experiment in which the rotor is spun for a time t_1 at an angle θ_1, then the magnetisation is stored along the z-axis while the spinner angle is hopped (≈ 30 ms), and finally coherence is transferred back to the central transition with rotor spinning at an angle θ_2. The two rotor axis angles are chosen in such a way that the conditions, Eq. (15),

$$P_2(\cos\theta_1) + P_2(\cos\theta_2) = 0$$
$$P_4(\cos\theta_1) + P_4(\cos\theta_2) = 0 \tag{15}$$

are satisfied. A simple DAS solution is $\{\theta_1, \theta_2\} = \{37.38^\circ, 79.19^\circ\}$.

Both DOR and DAS are technically very demanding and are limited by several factors. In the DAS experiment the T_1 relaxation time of the quadrupolar nuclei has to be larger than the hopping duration of the rotor. Spin exchange mediated by dipolar interaction can occur during the relatively long hopping time and an extra broadening might appear from large chemical shift anisotropies, since they are not completely averaged out. The DOR experiment is limited by the relatively slow spinning rates available thus producing a complex manifold of sidebands.

By manipulating the spin part of the Hamiltonian during MAS, *Frydman* and *Harwood* showed that a high-resolution NMR spectrum can be obtained by correlating multiple and single quantum coherences [11]. The technique was named multiple-quantum magic-angle spinning, MQMAS, and was introduced in 1995. Recently, using similar ideas, another method based on spin averaging was proposed by *Gan* called satellite transition MAS (STMAS) [13, 28]. In this experiment the single-quantum satellite transitions rather than the multiple-quantum transitions are correlated with the central transition. The main limitations of this technique seem to be the requirement for a very accurate setting of the magic angle (down to 0.1%) and the need for synchronised t_1 acquisition, which limits the available spectral widths. These issues are currently being investigated.

The rest of this review deals with MQMAS and its development. The ease in its implementation compared with DOR and DAS can be gauged from the numerous publications and applications that have resulted ever since its inception.

MQMAS-Principle and Practical Implementation

MQMAS is a 2D solid state MAS NMR experiment. It results in a high-resolution spectrum along the indirect dimension, correlated with its corresponding MAS spectrum in the detection dimension. This is achieved by simultaneously manipulating spin and spatial parts of the quadrupolar Hamiltonian. MAS takes the role of spatial averaging and removes the chemical shift anisotropy, CSA, the heteronuclear dipolar interactions, and the second rank elements of the second-order quadrupolar interaction. Radiofrequency pulses are used to manipulate the spin

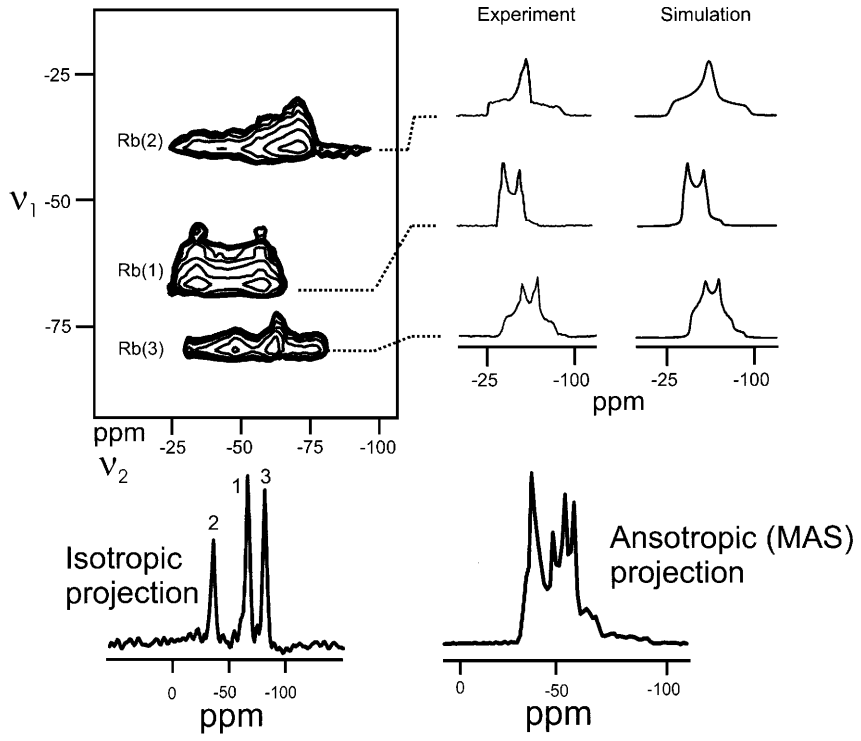

Fig. 4. Two-dimensional 3QMAS ^{87}Rb spectrum of $RbNO_3$ together with anisotropic slices corresponding to the three Rb sites from both experiment and simulations. Also shown are the isotropic and anisotropic projections, the former being the high-resolution quadrupolar spectrum and the latter corresponding to the normal MAS spectrum. The spectrum was recorded at a magnetic field of 4.7 T, MAS rate of 10.0 kHz, and rf strength of 70.0 kHz. The Rb sites are assigned both in the 2D spectrum and in the isotropic projection

part and average out the fourth rank elements of the second-order quadrupolar Hamiltonian. An echo is formed by correlating the frequencies of symmetric multiple-quantum coherences (MQC) and those of the central transition coherences (single-quantum coherence, SQC) for all crystallites in the powder simultaneously. Figure 4 shows a 2D ^{87}Rb MQMAS spectrum of a sample of polycrystalline rubidium nitrate. The isotropic projection (t_1 in time domain and F_1 or ν_1 in the frequency domain) clearly shows the three resolved ^{87}Rb sites. Sum projections on to the MAS dimension (t_2) of the three sites along with their corresponding simulations (theoretical lineshapes) demonstrate the possibility for obtaining the quadrupolar parameters.

Theory

Using Eq. (9), the evolution undergone by a $-m \leftrightarrow +m$ spin coherence can be expressed in terms of its accumulated phase ϕ given in Eq. (16) as [11, 12, 33]

$$\phi(m,\theta,\alpha,\beta,t) = \nu^{CS}2mt + \nu_Q^{(0)}C_0(I,m)t + \nu_Q^{(2)}(\alpha,\beta)C_2(I,m)P_2(\cos\theta)t + \nu_Q^{(4)}(\alpha,\beta)C_4(I,m)P_4(\cos\theta)t \quad (16)$$

where θ is the angle of rotation axis with respect to the static magnetic field, B_0. In the above ν^{CS} is associated with isotropic chemical shift. The C coefficients that depend on the spin quantum number I and the order of excited coherence, $M = 2m$, are given in Eq. (10). In a 2D experiment, spin coherences evolve during times t_1 and t_2. In order to obtain an isotropic echo signal, the anisotropic part of the phase ϕ should be set to zero. This can be done with the constraints in Eq. (17):

$$\begin{aligned}
&\nu_Q^{(2)}(\alpha,\beta)C_2(I,m_1)P_2(\cos\theta_1)t_1 + \nu_Q^{(2)}(\alpha,\beta)C_2(I,m_2)P_2(\cos\theta_2)t_2 = 0 \\
&\nu_Q^{(4)}(\alpha,\beta)C_4(I,m_1)P_4\cos(\theta_1)t_1 + \nu_Q^{(4)}(\alpha,\beta)C_4(I,m_2)P_4\cos(\theta_2)t_2 = 0. \qquad (17)
\end{aligned}$$

By setting $m_{1,2} = \frac{1}{2}$ (a single-quantum experiment) and the echo position to $t_2 = t_1$ all terms but those of Eq. (15) are eliminated, and the conditions for the DAS experiment are met. An alternative way to accomplish the same task is by manipulating the spin coherences, so that, by setting $\theta_1 = \theta_2 = \theta_{MA}$ and leaving $m_{1,2}$ as parameters, the above constraints reduce to Eq. (18) given by,

$$C_4(I,m_1)t_1 + C_4(I,m_2)t_2 = 0. \qquad (18)$$

Under these conditions, all 2nd rank anisotropies are removed, and since the expression above is independent of $\nu_Q^{(4)}$, all crystallites are refocused at a time $t_2 = -\frac{C_4(I,m_1)}{C_4(I,m_2)}t_1$ giving rise to a quadrupolar echo. This is the idea behind the MQMAS experiment.

In a MQMAS experiment, any order of MQC $2m_i$ can be used keeping in mind that the detection must be performed at the central transition. Thus, the experiment is performed by exciting MQC using a rf pulse and then converting them into single-quantum observable coherences using another rf pulse. However, recently *Jerschow et al.* showed that for a half-integer spin with $I > \frac{3}{2}$, higher order coherences can be correlated within each other, e.g. five-quantum (5Q) and triple-quantum (3Q) coherences, as long as an additional detection pulse is employed at the end of the sequence [34]. The MQ echo is picked up using a proper phase cycle and thus only the desired coherence pathway is selected. While experiments correlating MQ and SQ coherences are named 3QMAS, 5QMAS etc., the ones correlating various MQC's are named MQ/NQ MAS, where M and N are any two higher coherences. In principle, the highest resolution is attained by choosing the highest possible coherences [34, 35]. Thus, for a spin $\frac{5}{2}$, 3QMAS, 5QMAS and 5Q/3QMAS can all be performed with 5Q/3QMAS having the highest resolution.

Routinely, MQMAS is performed by correlating MQC with SQC giving rise to a purely isotropic second-order quadrupolar echo at a time

$$t_2 = \left| C_4(I,m_1)/C_4\left(I,\frac{1}{2}\right)\right| t_1. \qquad (19)$$

Since the ratio $\frac{C_4(I,m_1)}{C_4(I,\frac{1}{2})}$ can be of any sign, additional spin manipulation has to be performed in order to observe the echo, as will be discussed in the next section. A signal arising from a positive value of the ratio is called an echo and that arising from a negative value is called an antiecho. Table 1 gives the value of $k = \left|C_4(I,m_1)/C_4\left(I,\frac{1}{2}\right)\right|$ for various I and m values. Extension of this table to the MQ/NQ experiment is straightforward using the $C_l(I, m)$ coefficients in Eq. (10).

Table 1. The values of $k(I, m)$ in MQMAS

m/I	3Q	5Q	7Q	9Q
$\frac{3}{2}$	$\frac{7}{9}$			
$\frac{5}{2}$	$\frac{19}{12}$	$\frac{25}{12}$		
$\frac{7}{2}$	$\frac{101}{45}$	$\frac{11}{9}$	$\frac{161}{45}$	
$\frac{9}{2}$	$\frac{91}{36}$	$\frac{95}{36}$	$\frac{7}{18}$	$\frac{31}{6}$

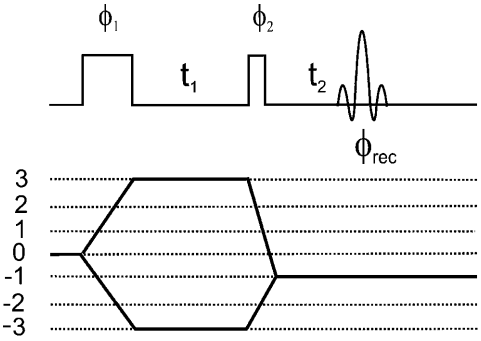

Fig. 5. The basic two-pulse (CW–CW) sequence used for MQMAS experiments along with the coherence pathways selected for 3Q experiments. The required phase cycle can be explicitly written as, $\phi_1 = 0°$, 60°, 120°, 180°, 240°, 300°, $\phi_2 = 0°$ and $\phi_{rec} = 0°$, 180°. (The same sequence may be used for 5QMAS with the following phase cycling: $\phi_1 = 0°$, 36°, 72°, 108°, 144°, 180°, 216°, 252°, 288°, 324°, $\phi_2 = 0°$ and $\phi_{rec} = 0°$, 180°. This phase cycling will select $0 \rightarrow \pm 5 \rightarrow -1$ pathways)

Pulse Schemes

The first MQMAS sequence as suggested by *Frydman* and *Harwood* consisted of three pulses, analogous to liquid state NMR sequences such as DQF-COSY and INADEQUATE [36, 37]. Based on the work of *Vega* and *Naor* on half-integer quadrupolar system (^{23}Na) [24] and *Vega* and *Pines* on double-quantum deuterium NMR [38], a two-pulse sequence was suggested by several authors independently [12, 39, 40]. The two-pulse scheme, Fig. 5, served as a foundation for subsequent developments in MQMAS. The first pulse excites all possible MQ coherences and the desired one is chosen by an appropriate phase cycling. After the MQ evolution the second pulse converts the MQC to 1QC resulting in an echo. In the two pulse scheme, the t_1 evolution time in the 2D experiment is governed solely by MQC evolution. Since the echo is formed at times $t_2 = kt_1$, it is tilted in the k direction leading to a time domain set as shown in Fig. 6a. Such a data set needs to be sheared to get a pure isotropic 2D *Fourier* transformed (FT) spectrum. The shearing is performed by employing a linear phase correction in the mixed (t_1, ν_2) domain [41]. The results of such a procedure is shown in Fig. 6(b–d). In order to obtain pure absorption 2D lineshapes, some modifications to the original sequence are needed and the three common methods are described in the following.

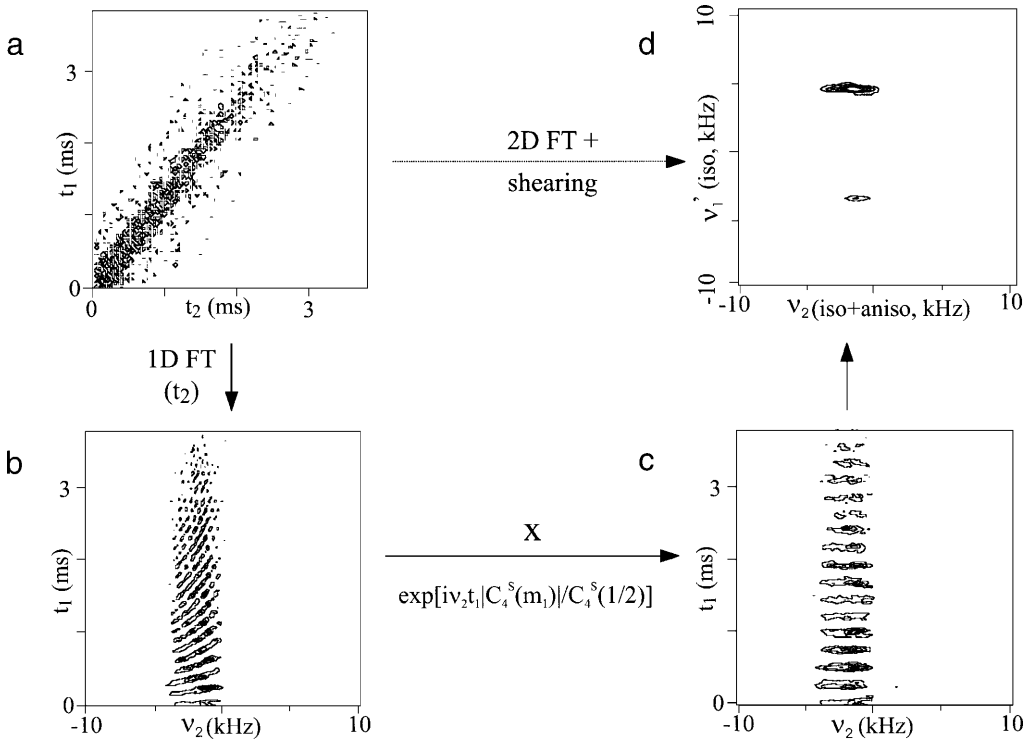

Fig. 6. Schematics showing the 2D time domain, shearing, and frequency domain representation of MQMAS spectrum: (a) $3Q \rightarrow 1Q$ correlation experiment obtained using the pulse sequence shown in Fig. 5. Note that the free induction decay, fid, has a slope of $\frac{7}{9}$ (Table 1). The shearing transformation is illustrated in (b) and (c) which is done via a first-order t_1-dependent phase correction along the F_2 axis (ν_2). (d) Isotropic $\rightarrow$ anisotropic correlation spectrum obtained after a *Fourier* and shearing transformation of the time-domain data set in (a). The spectrum corresponds to ^{23}Na 3QMAS of sodium oxalate, $Na_2C_2O_4$. The prime in (d) on ν_1 denotes the result after the shearing transformation. (Reproduced with permission from Ref. [12], Copyright (1995), American Chemical Society)

z-Filter Experiments

The z-filter was adapted to MQMAS from liquid state NMR [36] by *Amoureux et al.* [42]. This three pulse scheme (Fig. 7a) consists of a MQ excitation pulse, a mixing pulse that transfers $\pm m$ coherences into 0Q coherence, thereby introducing a z-filter and finally a soft 90° pulse that creates observable magnetisation ($m = -1$ coherence). The transfer of $(+m) \rightarrow (-1)$ and $(-m) \rightarrow (-1)$ does not occur with the same efficiency in the two-pulse experiment, Fig. 5. The middle pulse in the z-filter experiment forces an equal transfer by performing $\pm m \rightarrow 0$ coherence transfer. This scheme ensures a pure cosine modulation along the indirect dimension, t_1. Phase modulated data set in t_1 can be obtained by using hypercomplex acquisition or by employing TPPI/STATES [36]. The frequency spectrum is obtained by *Fourier* transforming along the direct dimension, F_2, performing a shearing transformation with a phase correction of $e^{ik\omega_2 t_1}$ of all points and again *Fourier* transforming along F_1, as demonstrated in Fig. 6.

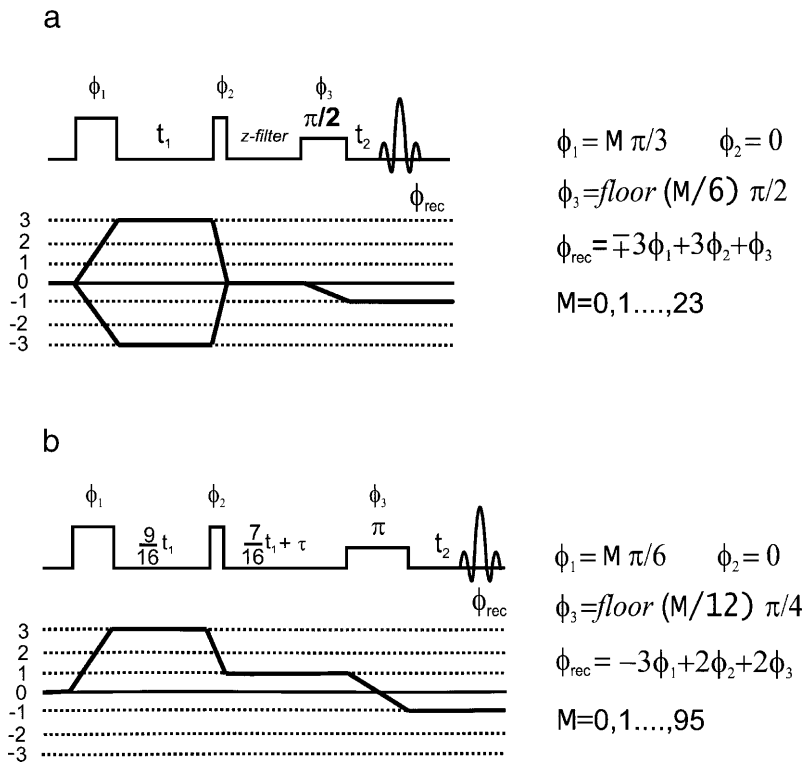

Fig. 7. MQMAS pulse sequences using (a) z-filter and (b) split-t_1 whole-echo scheme (this form of split-t_1 needs to be used for 3QMAS in spin-$\frac{3}{2}$) providing pure phase absorptive spectra with (b) avoiding the need for a shearing transformation. The phase cycle is mentioned in the figure. *floor*(x) returns the largest integer $\leq x$. In general, split-t_1 experiments have delays $\frac{1}{1+k}t_1$ and $\frac{k}{1+k}t_1$ which for spin-$\frac{3}{2}$ become $\frac{9}{16}t_1$ and $\frac{7}{16}t_1$

Phase-Modulated Split-t_1 Whole-Echo

Whole-echo acquisition [43], adapted to MQMAS by *Massiot et al.* [40], is an alternative way to obtain pure phase spectra. It relies on the fact that an echo of the fid can be induced by a π pulse without significant signal loss. *Fourier* transformation of such an echo signal leads to pure absorptive spectrum with a vanishing dispersive part, as long as relaxation effects are negligible.

The split-t_1 method, introduced by *Brown et al.* [44], gets rid of the need to do a shearing transformation by combining the MQ and 1Q (or NQ) evolution periods in the t_1 time domain. A combination with the whole-echo acquisition method results in a pure phase 2D MQMAS spectra, with ridges lying parallel to the F_2 frequency axis [45]. Figure 7b shows split-t_1 whole-echo pulse sequence for spin-$\frac{3}{2}$ where 3QC and 1QC evolve for times $\frac{9}{16}t_1$ and $\frac{7}{16}t_1$ respectively. These values correspond to the general required delays of $\frac{1}{1+k}$ for MQ evolution and $\frac{k}{1+k}$ for 1Q evolution.

The pulse sequence consists of three pulses: an excitation pulse, a conversion pulse and a soft π pulse to shift the echo. There are two different versions of this experiment, depending on the sign of $C_4(I, m_1)/C_4\left(I, \frac{1}{2}\right)$ (see Fig. 13). Since the echo always appears at a constant time during t_2, τ_{echo}, this time should be chosen

such that the whole echo appears in the fid. Signal processing includes: (1) putting the position of the echo signals at the middle of the fid's and zero filling symmetrically; a *Gauss*ian weighted window can be applied to the time domain data if desired, (2) redefining the time origin to be zero at the centre of the echo (this is similar to swapping the two halves of the spectrum), and (3) complex 2D FT (including apodisation, phasing etc.). An alternative approach includes (1) FT along t_1, (2) inversion of alternating points, and (3) FT along t_2.

Hypercomplex Experiments

Another method to obtain pure absorption line shapes is to collect a set of hypercomplex data. Two experiments are performed consecutively with a phase shift of $\frac{90^\circ}{M}$ on the first pulse, M being the order of coherence evolving during t_1. The resulting two signals, S_x and S_y, can be combined to yield echo and anti-echo signals by the following linear combinations:

$$\begin{aligned} S'_e(t_1, t_2) &= S_x - iS_y \\ S'_a(t_1, t_2) &= S_x + iS_y. \end{aligned} \tag{20}$$

A shearing transformation can now be applied after FT along F_2 (if needed):

$$\begin{aligned} S_e(t_1, w_2) &= e^{ikw_2t_1} S'_e(t_1, w_2) \\ S_a(t_1, w_2) &= e^{-ikw_2t_1} S'_a(t_1, w_2). \end{aligned} \tag{21}$$

The FT will create two sets of 2D signals which can be combined according to

$$S(w_1, w_2) = S_e(w_1, w_2) + S_a(-w_1, w_2) \tag{22}$$

thus giving rise to pure absorption mode lineshapes.

Additional Pulse Scheme Combinations

In addition to the three schemes mentioned above, several other pulse combinations may be considered. A z-filter sequence can be combined with split-t_1 experiments by using the following coherence pathway: $\pm 3 \rightarrow \pm 1 \rightarrow 0 \rightarrow -1$. This makes use of 4 rf pulses, the first two hard rf pulses for excitation of MQC and their conversion to ± 1 coherences. The latter two are soft $\pi/2$ pulses. Another option is to perform a split-t_1 experiment without shifting the echo. In this case a hypercomplex acquisition should be performed, without the need for a shearing transformation. Sometimes such combinations can be advantageous, since sensitivity enhancement schemes, which will be discussed later, can be successfully applied to them.

Data Analysis – Extraction of NMR Parameters

After applying the *Fourier* transformation, the axes have to be properly labelled and referenced according to the experimental conditions. The labelling scheme corresponds to either the split-t_1 frequency domain data, or to a sheared MQMAS spectrum. This labelling is not straightforward since the evolution in the F_1 domain is governed by isotropic chemical and second-order quadrupolar shifts.

There are several different ways in the literature to label the axes [46, 47]. We adopt here a method in which the apparent *Larmor* frequency does not scale with M

(the order of MQ coherence evolving during t_1), but its sign can change according to the specific experiment. A negative *Larmor* frequency is used (*i.e.* the isotropic axis is inverted before any referencing is performed) if $M<2I$, and positive otherwise. Referencing the spectrum along the F_1 dimension should take into account the evolution of the isotropic chemical shift (δ_{cs}) under MQ and 1Q coherences. The reference frequency in F_1 is defined therefore as $\frac{k-M}{1+k}\delta$, δ being the shift in ppm with respect to a reference sample. This expression is the sum of $\frac{-M}{1+k}\delta$, chemical shift resulting from the evolution of MQC's, and $\frac{k}{1+k}\delta$, chemical shift resulting from the evolution of single-quantum coherence. The expressions for δ_1 (frequency shift in ppm along F_1) and δ_2 (centre of gravity of peaks along F_2) depend on δ_{cs} and on the second order quadrupole shift (δ_Q) and are given by Eq. (23) and Eq. (24) as [48],

$$\delta_1 = \frac{-p+k}{1+k}\delta_{cs} + \frac{A(I,p) - kA(I,-1)}{1+k}\delta_Q \tag{23}$$

$$\delta_2 = \delta_{iso} + A(I,-1)\delta_Q \tag{24}$$

where

$$A(I,p) = \frac{p}{30}(4I(I+1) - 3p^2). \tag{25}$$

The values of k are given in Table 1 and $p=-M$ for a coherence order $M=2I$, $p=M$ for $M<2I$. The centre of gravity is generally defined as in Eq. (24)

$$\delta_2 = \frac{\int \nu_2 I(\nu_2) d\nu_2}{\int I(\nu_2) d\nu_2}. \tag{26}$$

When the lineshapes are clearly resolved in the 2D spectra, each site can be projected separately by taking the sum of relevant slices. The quadrupolar parameters can be either simulated or extracted by moment analysis [49] or direct calculation [50]. When distributions of quadrupolar interactions and chemical shifts exist, lineshapes cannot always be properly defined. This situation is encountered many times in substances like glasses, ceramics and mesoporous materials. In such cases, the extraction of the NQCC and η is cumbersome, but it is still possible to obtain the value of the second order quadrupole effect $\left(\text{SOQE} \equiv \chi\sqrt{1+\eta^2/3}\right)$. The values of δ_{cs} and SOQE can be extracted by inverting Eqs. (23) and (24), resulting in Eq. (27) and Eq. (28),

$$\delta_{cs} = -\frac{(1+k)A(I,-1)}{pA(I,-1)+A(I,p)}\delta_1 + \frac{A(I,p)+kA(I,-1)}{pA(I,-1)+A(I,p)}\delta_2 \tag{27}$$

$$\delta_Q = \frac{1+k}{pA(I,-1)+A(I,p)}\delta_1 + \frac{p-k}{pA(I,-1)+A(I,p)}\delta_2, \tag{28}$$

with

$$SOQE = \frac{\omega_0/2\pi}{10^3}\sqrt{\delta_Q}\times\frac{4I(2I-1)}{3}. \tag{29}$$

An alternative approach for the extraction of the NMR parameters is by performing MQMAS at two different magnetic fields, and comparing only the values of δ_1 along the F_1 frequency axis.

Experimental Aspects

Optimisation of MQMAS pulse sequence starts with a proper calibration of the rf power, so that selective pulses (selective 90° and 180°) could be employed accurately for z-filter or shifted echo experiments. This is done with a reference sample, usually a solution, where ν_Q is averaged to zero.

The MQMAS excitation and conversion pulses are then adjusted by monitoring the MQ echo intensity in a one-dimensional (1D) experiment, employing a very small delay, between the excitation and conversion pulses, of say, 5 μs. Initially, the excitation pulse is fixed to some value and the duration of the conversion pulse is varied. Then, the length of the excitation pulse is varied for the optimised conversion pulse length. The optimisation protocol can be usually accomplished on a sample of Na_2SO_4 or Na_2ClO_3 for spin-$\frac{3}{2}$ systems and aluminium acetyl acetonate for spin-$\frac{5}{2}$ systems, but it may be noted here that the optimum values are ν_Q dependent, Fig. 8.

Starting values for the pulses can be obtained from numerical simulations as illustrated in Fig. 8. Figure 8a shows the maximum 3QC intensity that could be obtained for various quadrupolar strengths as a function of the pulse duration with the rf field fixed at 95 kHz. In b, the efficiency of the 3Q → 1Q conversion pulse is

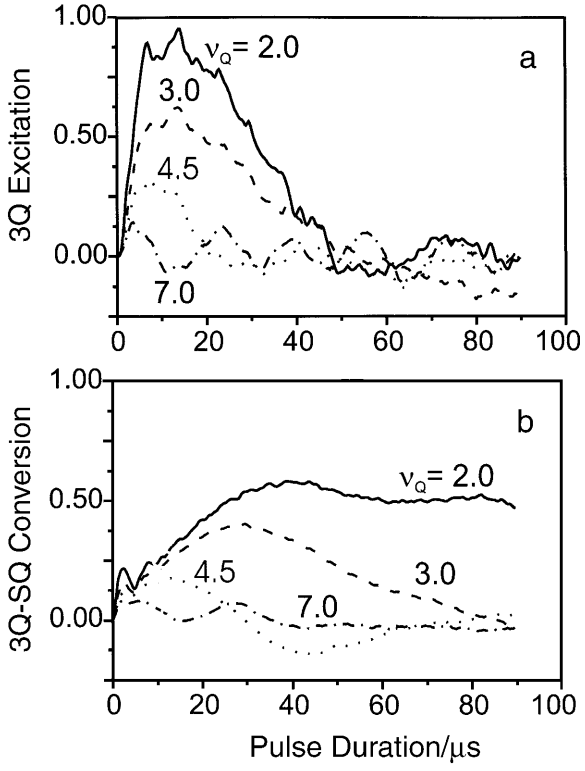

Fig. 8. (a) Plot of the 3Q intensity as a function of the duration of the pulse (excitation pulse in a MQMAS scheme) for various values of ν_Q and (b) plot of the SQ intensity as a function of the duration of the pulse (conversion pulse in a MQMAS scheme) for $\nu_1 = 95$ kHz, and MAS rate of 8 kHz. Three hundred powder orientations were considered for the simulation

indicated for each of the values of NQCC calculated in a. It may be emphasised here that the overall excitation efficiencies achieved by the optimised pulses are 62% and 33% for NQCC of 3.0 and 4.5 MHz with the amount of the 1QC eventually obtained being around 40% and 18%. The values are relative to the theoretical MAS single quantum signal and they already point to the main weakness of this method, which is the lack of an appreciable sensitivity.

In order to perform a successful and useful MQMAS experiment three steps need to be taken. They are (1) choosing a proper pulse scheme for pure phase spectroscopy, (2) selecting a suitable enhancement scheme to improve the sensitivity of the excitation and conversion pulses, and (3) optimisation of all the pulses. A pulse scheme should be chosen by taking into account several factors, some of which were already mentioned previously (relaxation times and spin quantum number) but also factors like the gyromagnetic ratio and the hardware capabilities. Some of these factors are crucial when choosing the right sensitivity enhancement scheme and will be elaborated on extensively in the next section.

Sensitivity Enhancement in MQMAS

In Fig. 8 it was shown that the excitation and conversion processes are inherently inefficient using hard pulses. The excitation efficiency of 3QC, for example, drops as $\frac{\nu_1^2}{\nu_Q^2}$. Some of the most important applications of MQMAS are envisaged in systems in which low-γ nuclei like ^{17}O, which is of low natural abundance also, can be probed routinely. It has also been established that a correlation of the highest possible MQC to 1QC achieves the best resolution, and if possible, MQC to NQC. However, excitation of 5QC, 7QC, 9QC in higher spin systems is even more difficult compared with the 3QC excitation. Figure 9 shows the amount of 3QC generated for a typical quadrupolar system for rf values of 50 kHz (a) and 100 kHz (b) as a function of the pulse duration for several MAS rates [51]. Although, high rf values (and high MAS for better lineshapes) are attractive with higher values of the NQCC, the required rf fields and MAS rates are out of reach in most of the spectrometers. Signal-to-noise can be gained by synchronous detection [52] or by acquiring multiple echoes during the free precession of the observable magnetisation (QCPMG) [53], but the gains achieved are not appreciable. The following sections demonstrate how a manipulation of the rf pulses can lead to significant signal gain which could of course be combined with the schemes mentioned above. The noticeable effect on the lineshapes is also discussed.

Enhancement Schemes for Spin-$\frac{3}{2}$

The first attempt to enhance 3Q excitation efficiency was by *Marinelli et al.* [54] making use of composite pulses. They showed that an application of two hard pulses with a 90° phase difference, and nutation angles of θ and 2θ for the first and second pulse respectively, resulted in an enhancement of the order of 30% in spin-$\frac{3}{2}$ systems. The flip angle θ needs to be optimised according to the rf power and quadrupolar strength. For sodium oxalate using $\frac{\nu_Q}{\nu_1} = 17$, for instance, the best 3QC was obtained with $\theta \approx \pi/2$. When large chemical shift anisotropies exist, such as

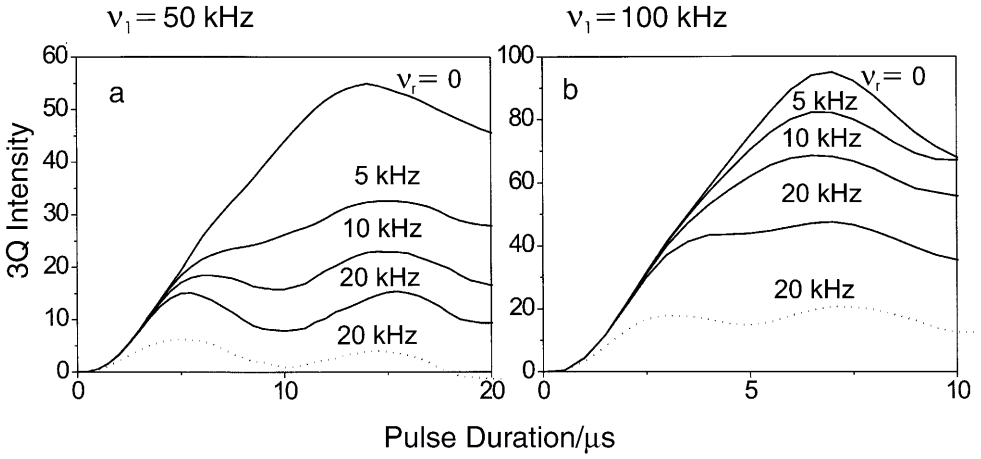

Fig. 9. Plot of the 3Q intensity (normalised with respect to single-quantum MAS signal) as a function of the duration of the pulse (excitation pulse in a MQMAS scheme) for (a) $\nu_1 = 50\,\text{kHz}$ and (b) $\nu_1 = 100\,\text{kHz}$ for various MAS rates, ν_r indicated on the top of each curve. The following quadrupolar parameters, $\nu_Q = 2.50\,\text{MHz}$ and $\eta = 0.70$, were assumed for the simulations except for the dotted curve for which $\nu_Q = 5.0\,\text{MHz}$ and $\eta = 0.70$

the case for a spin-$7/2$ ^{59}Co complex, a $x\bar{x}$ composite pulse proved to be more efficient, but flip angles can no longer be predicted in a simple manner.

A significant step towards enhancing the MQMAS signal was made with the introduction of the RIACT-II (rotation induced adiabatic coherence transfer) scheme [55] (Fig. 10a). Here the excitation pulse consists of a selective 90° pulse creating central transition coherences, immediately followed by a long hard CW pulse, $1/4$ of a rotor period (τ_r) in length. For the conversion pulse again a pulse of duration $\tau_r/4$ is used. Another advantage of this scheme is its ability to perform equally well on a relatively large range of quadrupolar constants, thus making MQMAS more quantitative. However, the main drawback of the experiment is the distortion of the lineshapes along the MAS dimension [56]. It has been shown that moving the position of the rf offset has a substantial effect on the pulse efficiency. Hence, it can be used to selectively excite certain sites according to their quadrupolar strengths, while minimising the intensity of others [57], and thus may be used as a spectral editing technique.

The RIACT approach was soon followed by an experimental scheme using modulated rf fields for conversion of MQC to SQC. Two variants were introduced, namely, double frequency sweeps, DFS, Fig. 10(b) [58] and fast amplitude modulation, FAM, Fig. 10c [59, 60]. The resulting signal enhancement was approximately 3-fold relative to the original two-pulse (CW–CW) scheme (Fig. 5 or Fig. 7b, the split-t_1 version) depending on the quadrupolar strength. While DFS uses continuous modulation of the rf frequency, FAM utilises a discreet single amplitude modulation frequency. Their major advantage over the RIACT-II scheme (having approximately the same signal enhancement) is the improved lineshapes along the MAS dimension, thereby allowing more accurate determination of NQCC and η. Both DFS and FAM are ν_Q dependent.

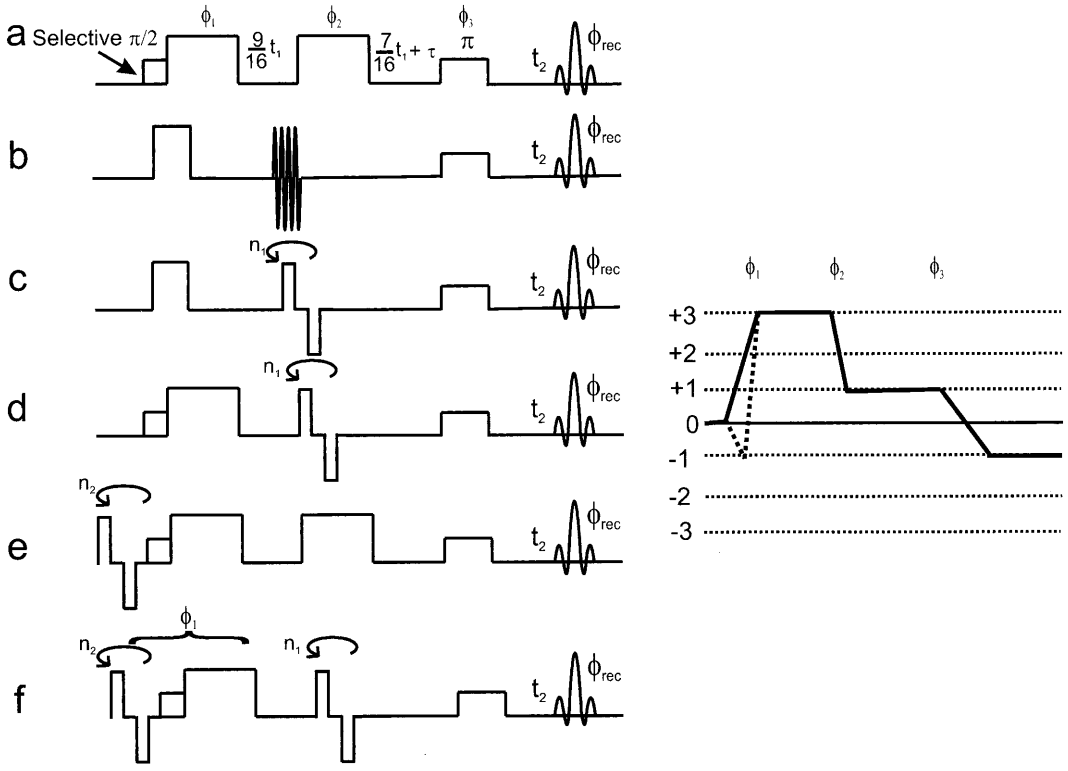

Fig. 10. Sensitivity enhanced MQMAS pulse schemes for spin-$\frac{3}{2}$ with split-t_1 whole-echo acquisition: (a) RIACT, (b) DFS, (c) FAM-I, (d) RIACT-FAM-I, (e) FAM-I-RIACT, and (f) FAM-I-RIACT-FAM-I sequences. The coherence pathways (dotted pathway for a, d, e, and f) selected for each of the schemes are the same as indicated in the figure; n_1 and n_2 are the number of times the FAM-I loop is repeated, with n_2 often equalling a full rotor period. Both $\frac{\pi}{2}$ and π pulses are soft pulses

The DFS pulses require an rf field strength of the order of 100–150 kHz. Diverging rf frequency sweeps are employed covering the whole ν_Q range. With no previous knowledge of the quadrupolar strengths, a sweep of over ≈ 2.5 MHz should be used, as this is normally the practical bandwidth of the probe. The sweep should start at a slightly off-resonance carrier frequency, starting with zero amplitude or half-Gaussian shape at the beginning of the pulse. Finally, one needs to optimise the sweep length. When the sweep covers the whole range of ν_Q values, an optimum length is approximately a quarter of a rotor period. These are starting values which can be further optimised [58, 61, 62].

FAM pulses, lately referred to as FAM-I, employ standard rf fields ($\nu_1 = 70$–110 kHz), and are designed from a repeating unit of four segments: a pulse with a positive phase, a delay, a pulse with a negative phase and a final delay $[\tau_x, \tau, \tau_{\bar{x}}, \tau]_n$, n is the number of repetitions). Optimisation is done by setting $\tau = 1$ µs, and $n = 4$. The values of n, τ are varied until maximum echo intensity is obtained in the 1D experiment. Variation of the basic FAM block can be made by adding several units with different n and τ numbers (extended FAM-I [63]), or by changing the lengths of the pulses with respect to the delays. The first option can be viewed as the discreet and simplified version of the DFS pulses. A major outcome of the introduction of

these modulated rf schemes was the gaining of a better understanding of the MQC to SQC conversion process and of the characteristics of echo formation [60, 63]. This latter understanding resulted in the SL-FAM scheme, Fig. 10d (hereafter referred to as RIACT-FAM), obtained by combining RIACT excitation and extended FAM-I conversion, resulting in high sensitivity, relatively undistorted lineshapes and reduced dependence on NQCC.

With FAM-I it is possible to redistribute the population of the spin energy levels. This is called RAPT (rotor assisted population transfer) [64]. It has been shown that an enhancement by a factor of 1.5–2 is achieved in a MAS experiment on spin-$\frac{3}{2}$, when satellite redistribution is achieved before the excitation pulse, as shown in Fig. 11. The RAPT experiment comprised of the basic FAM-I scheme, $[\tau_x, \tau, \tau_{\bar{x}}, \tau]_n$, where the value of n is set to a large number such that the modulation lasts for a whole rotor period. The pulses are normally set to 1 µs and delays to the shortest time possible subjected to the hardware capabilities (e.g. transmitter phase stabilisation). However, shortening the delays is not very crucial for the performance of this scheme. The theoretical enhancement is $I + \frac{1}{2}$ if a complete satellite

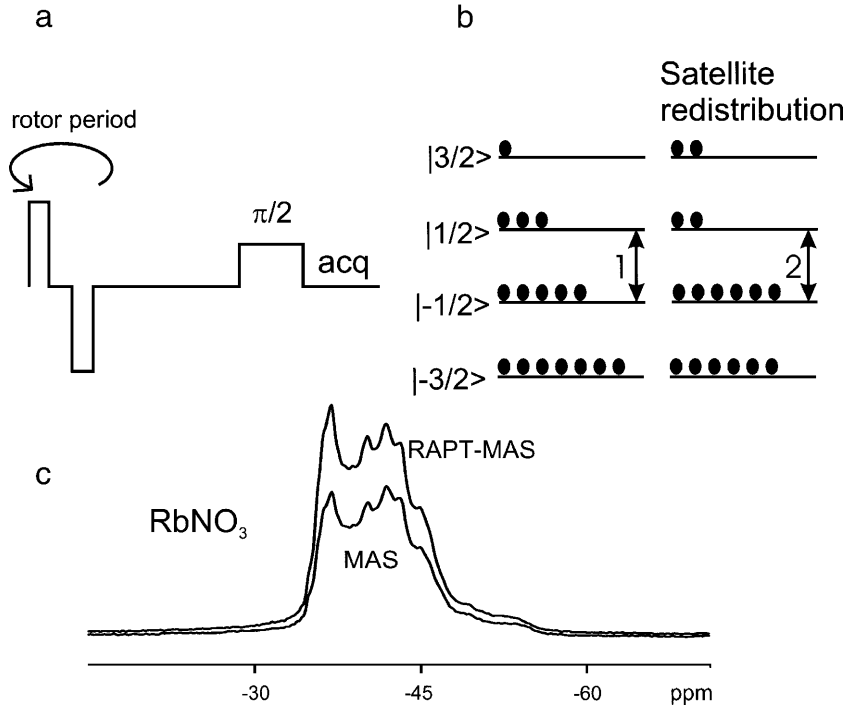

Fig. 11. (a) Pulse sequence used for the FAM-MAS experiment (RAPT scheme) employing FAM pulses lasting for a full rotor period followed by a soft $\frac{\pi}{2}$ pulse. (b) Population arrangement for a spin-$\frac{3}{2}$ system at thermal equilibrium (left) and after satellite redistribution with FAM pulses (right, one possible arrangement involving saturation of satellite transitions). (c) A single-pulse MAS spectrum and the corresponding FAM-MAS spectrum of a sample of $RbNO_3$. An enhancement by a factor of ≈ 1.8 was obtained with a spinning rate of 10.0 kHz and a FAM block given by [1 µs (pulse, x phase), 1 µs (delay), 1 µs (pulse, $\bar{x}$ phase), 1 µs (delay)], repeated 25 times lasting 100 µs. The external magnetic field was 4.1 T

saturation is achieved. The schematic in Fig. 11 corresponds to complete satellite saturation.

It is possible to combine RAPT with a MQMAS sequence that utilises SQC for the excitation of MQC and obtain an additional signal gain. The combination of RAPT and RIACT-II is shown in Fig. 10e [65]. A combination of RAPT with RIACT-FAM (FAM-RIACT-FAM) [66], Fig. 10f, gives the best performance so far for the MQMAS experiments in spin-$\frac{3}{2}$ systems, in terms of signal-to-noise and lineshapes.

Figure 12 shows the isotropic projection, anisotropic projection and a slice through one of the quadrupolar sites of a sample of $RbNO_3$ obtained by the use of six MQMAS schemes, namely, CW–CW, RIACT-II, CW-FAM-I, RIACT-FAM-I, FAM-RIACT-II and FAM-RIACT-FAM. Indeed, the last scheme provides the highest signal-to-noise ratio and the least distortions in the second-order quadrupolar

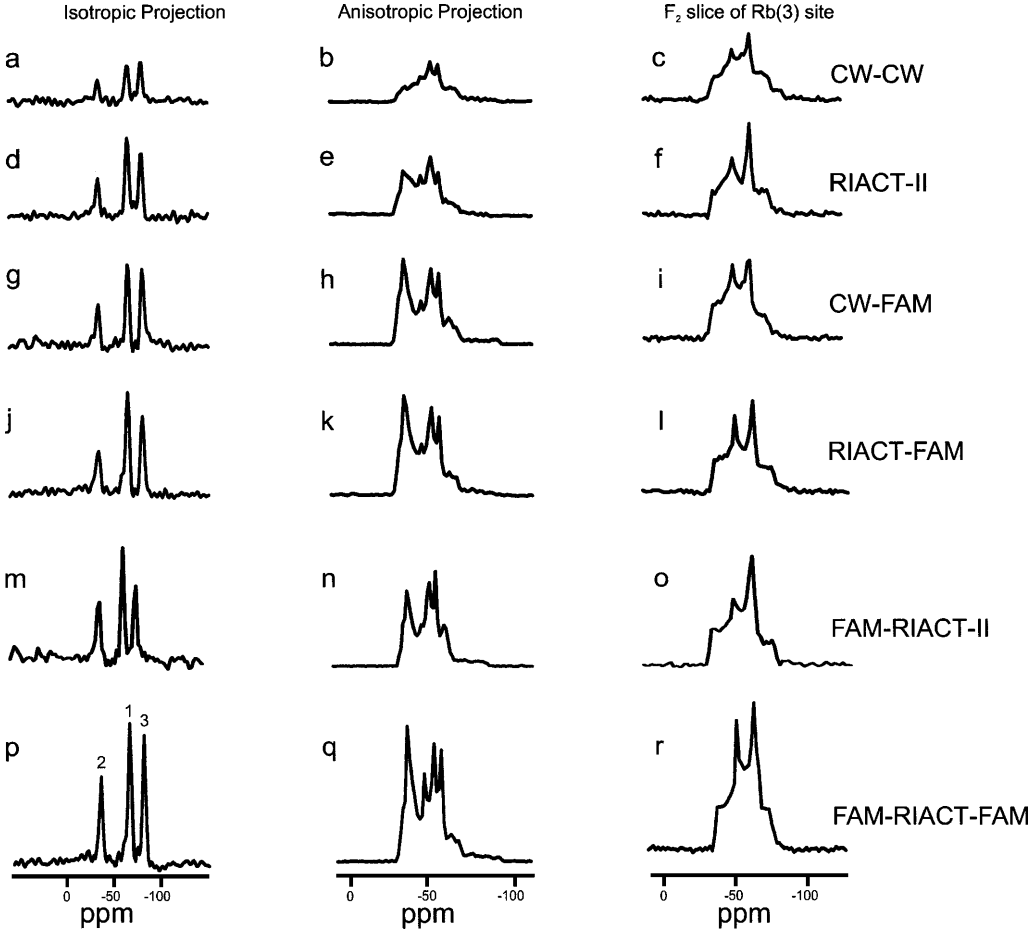

Fig. 12. Isotropic projection, anisotropic projection and an anisotropic slice across the Rb(3) site of $RbNO_3$ obtained from the pulse sequences CW–CW, RIACT, FAM-I, RIACT-FAM-I, FAM-I-RIACT and FAM-I-RIACT-FAM-I. For the experiments, an external magnetic field of 4.7 T, $\nu_r = 10.0$ kHz, hard pulses with a rf strength of 70.0 kHz, and soft pulses with a strength of 20.0 kHz were used. (Reproduced with permission from Ref. [66])

lineshapes. (No comparison was made with DFS scheme as a conversion pulse, however it is expected to perform at least equally as well as the FAM-I scheme).

FAM-I, DFS and RIACT use an adiabatic anti-crossing mechanism in order to efficiently convert the 3QC to the 1QC, th details of which are extensively dealt with in Ref. [60, 62].

A different approach to obtain sensitivity enhancement was suggested by *Vosegaard et al.* [67]. Two long pulses with a duration of 2–3 rotor periods were applied to the quadrupolar spins, employing low rf fields and high spinning rates. Rotary resonance conditions were found, in which an excitation minimum occurs when $2\omega_1 = n\omega_r$, $(n = 0,1,\ldots)$ and in between those minima points, enhanced signals were obtained. For the conversion pulse a maxima was found at $\omega_1 = n\omega_r$. This scheme called FASTER-MQMAS experiment achieves a 3-fold enhancement of the MQMAS spectra (like FAM-I, although at a lower rf power), but provides distorted lineshapes, as the excitation and conversion pulses select only a specific portion of the crystallites. A spectrum of $RbClO_4$ was obtained with a spinning rate of 30 kHz, an excitation pulse of duration $\tau = 75\,\mu s$ (2.25 rotor periods) and rf power $\nu_1 = 37$ kHz and a conversion pulse with $\tau = 65\,\mu s$ (1.95 rotor periods) and $\nu_1 = 30$ kHz. The selective echo π pulse was employed at $\nu_1 = 30$ kHz.

Enhancement Schemes for Spin-$\frac{5}{2}$

Spin-$\frac{5}{2}$ systems are more complex than spin-$\frac{3}{2}$ systems in the sense that additional energy levels are involved during the process of excitation and conversion. This fact complicates the rather simple mechanisms that explained the enhancement phenomena in spins-$\frac{3}{2}$. Thus, enhancement schemes for spin-$\frac{5}{2}$ based on the same design as spin-$\frac{3}{2}$ do not perform equally well.

Sensitivity enhancement of 3QMAS and 5QMAS spectra in spin-$\frac{5}{2}$ was obtained by employing FAM-I pulses for conversion of MQC to SQC [68]. *Iuga et al.* [61] have shown that a very accurate lineshape of a $\chi = 15.3$ MHz ^{27}Al site of the mineral andalusite could be obtained using DFS pulses from a 3QMAS spectrum. They also obtained some signal enhancement in the 5QMAS spectra of $9Al_2O_3 \cdot 2B_2O_3$ using DFS pulses, but with strong lineshape distortions [61]. Considerable shortening of the FAM-I pulse, up to a composite pulse scheme (FAM-II, Fig. 13a) [69] has been shown to enhance the 3QMAS signal of $AlPO_4$-5. This very short scheme makes FAM-II independent of the spinning rate. The same idea was exploited for the signal enhancement in 5QMAS experiments (Fig. 13b), where FAM-II was incorporated in the excitation pulse and either FAM-I or FAM-II used for conversion of 5QC to SQC [48]. A subtle point to be noted in Fig. 13a and b is the difference in the way split-t_1 scheme is executed for 3QMAS and 5QMAS in spin-$\frac{5}{2}$ systems. In general, for a correlation of the highest MQC with 1QC, a scheme like Fig. 13b needs to be chosen, while for a correlation of all the lower coherences with the SQC, a scheme like Fig. 13a is the desired one. FAM pulse scheme can not be efficiently incorporated into the original version of the z-filter scheme, but rather in a modified version in which the z-filter follows a split-t_1 procedure.

FAM-II is essentially composed of several pulses with alternating phases. The overall duration of a FAM-II pulse is short, up to $\approx 5\,\mu s$. A starting unit for $3Q \rightarrow 1Q$

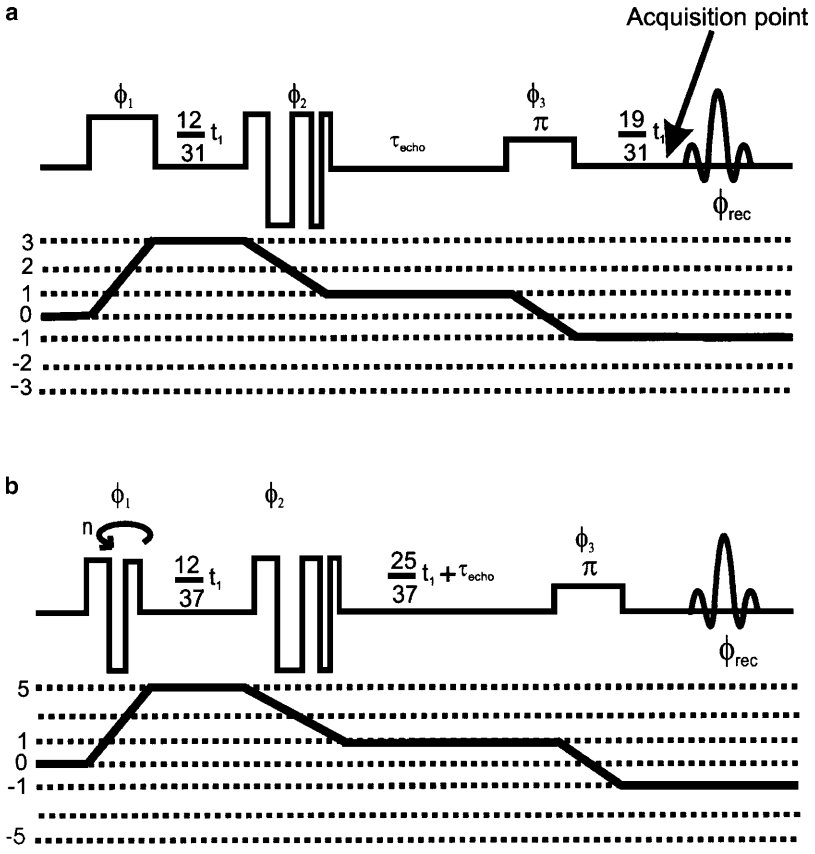

Fig. 13. (a) FAM-II split-t_1 whole-echo pulse sequence used for sensitivity enhancement in the 3QMAS of spin-$\frac{5}{2}$ systems. The acquisition starts after a delay of $\frac{19}{31}t_1$ (where the arrow points to). (b) CFF (CW-FAM-FAM) split-t_1 whole-echo pulse sequence used for the 5QMAS of spin-$\frac{5}{2}$ systems with FAM-II kind of approach employed for enhancing both excitation and conversion efficiency

conversion can be 2, $\bar{1}$, 0.5 μs. (A bar means a negative phase, numbers correspond to pulse durations). Addition or subtraction of segments, as well as length variations should be performed according to spectrometer capabilities, since transmitter phase glitches introduce pulse distortions.

In a 5QMAS experiment, a short $[x\bar{x}]_n$ modulation (FAM-II) is applied following a hard excitation pulse with optimised values of n and pulse durations. The hard excitation pulse creates 3QC from the equilibrium population and FAM-II converts the 3QC to 5QC. For conversion (5QC-SQC), a two-part FAM-I pulse or a two-part FAM-II pulse can be used. *Vosegaard et al.* suggested, for the first and second parts of a FAM-1 pulse, values of 0.4 and 0.85 μs and n of 6 and 4 [68]. A FAM-II pulse for conversion may be optimised from a series of pulses of the initial form $2, \overline{1.5}, 1, \overline{0.5}, 1.5, \bar{1}$.

Without loss of generality, it may be stated that FAM-I pulses are preferred for conversion of the highest MQC to 1QC, as this process is always adiabatic [60]. For all other MQC → 1QC, FAM-II pulses are preferred.

Although none of the enhancement schemes have been reported on higher spin systems (except for one example on cobalt, spin-$\frac{7}{2}$ [54]), it is reasonable to believe

Table 2. The phase table for 3Q- and 5QMAS split-t_1 whole-echo sequences

Experiment	Phase	Value/degrees
3QMAS	ϕ_1	$(0, 30, 60, 90, 120, 180, 210, 240, 270, 300, 330)_8$
	ϕ_2	$(0)_{96}$
	ϕ_3	$(0)_{12}$, $(45)_{12}$, $(90)_{12}$, $(135)_{12}$, $(180)_{12}$, $(225)_{12}$, $(270)_{12}$, $(315)_{12}$
	ϕ_{rec}	$\{(0, 270, 180, 90)_3, (90, 0, 270, 180)_3, (180, 90, 0, 270)_3, (270, 180, 90, 0)_3\}_2$
5QMAS	ϕ_1	$(0, 18, 36, 54, 72, 90, 108, 126, 144, 162, 180, 198, 216, 234, 252, 270, 288, 306, 324, 342)_8$
	ϕ_2	$(0)_{160}$
	ϕ_3	$(0)_{20}$, $(45)_{20}$, $(90)_{20}$, $(135)_{20}$, $(180)_{20}$, $(225)_{20}$, $(270)_{20}$, $(315)_{20}$
	ϕ_{rec}	$\{(0, 270, 180, 90)_5, (90, 0, 270, 180)_5, (180, 90, 0, 270)_5, (270, 180, 90, 0)_5\}_2$

that a gain in signal-to-noise could be obtained by using one or several of the above mentioned schemes.

We conclude this section by giving the explicit phase cycle values, Table 2, for split-t_1 shifted-echo 3QMAS (Fig. 7b, 10, 13a) and 5QMAS (Fig. 13b, 13c) sequences.

Heteronuclear Experiments Involving MQMAS

With MQMAS as a high-resolution solid state NMR tool, one may design heteronuclear experiments which lead to connectivity information, distance measurements and additional spectral editing techniques. Spin-locking of half-integer quadrupolar spins is hard to achieve. However, when the *Hartmann-Hahn* condition, $\omega_{S,nut} = \omega_{I,rf} \pm n\omega_r$ (n being an integer), is met, instances can be found in which cross-polarisation (CP) becomes possible to some extent [6, 7]. Several schemes have been proposed that combine CP with MQMAS. Initially it was suggested to cross-polarise ^{19}F to ^{27}Al [70] or ^{1}H to ^{27}Al [71] employing a very low rf field on the ^{27}Al channel, $\nu_{1S} = 5$ kHz, and to detect the z-filtered 3QMAS spectra of the ^{27}Al nucleus. These CP-MQMAS experiments gave very poor signal-to-noise ratio. While a normal 3QMAS experiment took appromimately 30 minutes to collect, a ^{27}Al{^{1}H}CP version had a poor signal intensity even after 16 hrs. Nevertheless, connectivity information could be obtained, thus providing spectral editing possibilities.

The efficiency of these experiments was improved by two different approaches. The first one uses again single-quantum cross-polarisation, combines the CP step with an inverse split-t_1 MQMAS experiment, which could incorporate FAM pulses to gain even more signal-to-noise [72]. The second one employs cross-polarisation directly to the triple-quantum transitions [73]. It was also demonstrated that any multiple-quantum transition can in principle be cross-polarised under suitable conditions [74, 75].

The cross-polarisation process was utilised to perform a MQMAS/HETCOR experiment [76], in which ^{23}Na polarisation was transferred to a ^{31}P nucleus after

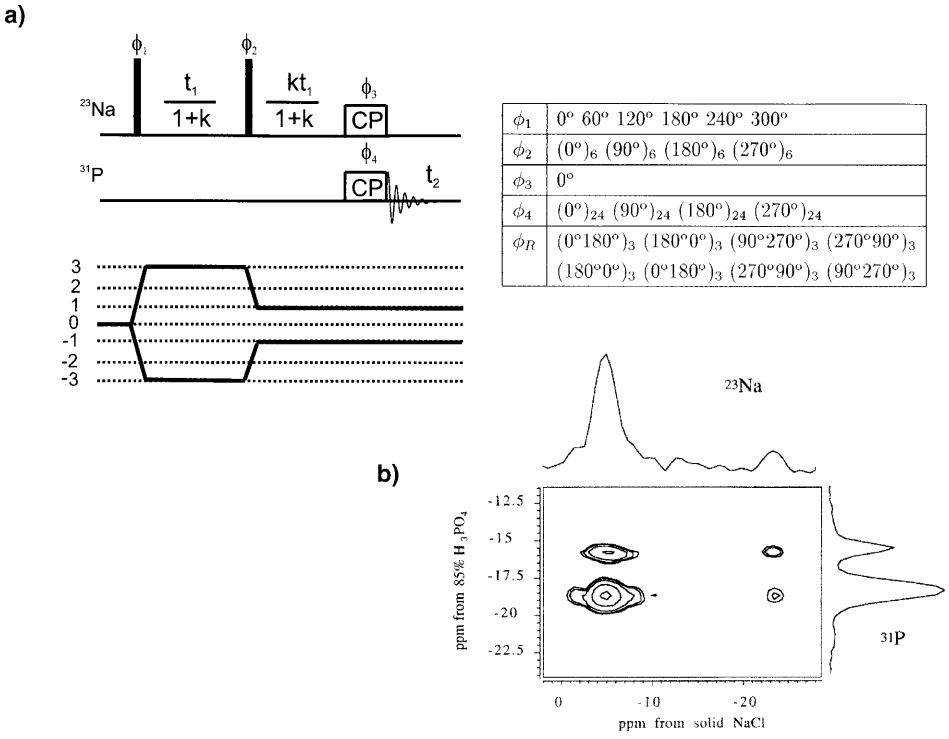

ϕ_1	0° 60° 120° 180° 240° 300°
ϕ_2	$(0°)_6$ $(90°)_6$ $(180°)_6$ $(270°)_6$
ϕ_3	0°
ϕ_4	$(0°)_{24}$ $(90°)_{24}$ $(180°)_{24}$ $(270°)_{24}$
ϕ_R	$(0°180°)_3$ $(180°0°)_3$ $(90°270°)_3$ $(270°90°)_3$ $(180°0°)_3$ $(0°180°)_3$ $(270°90°)_3$ $(90°270°)_3$

Fig. 14. (a) Pulse sequence, coherence transfer pathways and phase cycle table for MQMAS/HETCOR experiment. To obtain 2D pure-absorption line shapes both $+3$ and -3 pathways are retained. The 96 step phase cycle is such that both CYCLOPS [96] and spin-temperature alternation [97] are incorporated. The phase of ϕ_3 needs to be shifted by 90° to include STATES procedure. (b) ^{23}Na–^{31}P MQMAS-HETCOR spectrum of $Na_3P_2O_9$. The external magnetic field corresponded to a proton frequency of 500 MHz, the two pulses in (a) were 16 μs long corresponding to a 3π rotation on the central transition of ^{23}Na, CP contact time was 10 ms and $\nu_r = 5$ kHz. Thirty five complex t_1 increments were collected each consisting of 960 transients with a recycle delay of 3 s. (Reproduced with permission from Ref. [76])

performing a split-t_1 MQMAS experiment with amplitude modulated data set. In Fig. 14 an example of the pulse sequence and the corresponding spectrum is given. The advantage in transferring ^{23}Na magnetisation to ^{31}P in the sample of $Na_3P_3O_9$ and not *vice versa* stems from the relatively short T_1 of the ^{23}Na (3 s) compared with that of ^{31}P (600 s).

The rotational echo double resonance (REDOR) experiment [77] probes the distance between two spin-$\frac{1}{2}$ nuclei. It is possible to probe the distance to a quadrupolar nucleus by performing REAPDOR [78]. However, in this experiment, the quadrupolar spin is not directly detected. By applying REDOR decay pulses during SQ evolution (MQ-t_2-REDOR) [79] or during MQ evolution (MQ-t_1-REDOR) [80] of a MQMAS experiment, distances can be probed between a quadrupolar nucleus and a spin-$\frac{1}{2}$ nucleus, while detecting the quadrupolar spin. Application of the REDOR pulses during 3QC evolution, for instance, enhances the dipolar interaction by a factor of 3, thus enhancing the sensitivity of the experiment. Figure 15 demonstrates the applicability of the experiment on a sample of $AlPO_4$-CHA. The

pulse sequence for (a) MQ-t_2-REDOR and (b) MQ-t_1-REDOR are shown, with a fit of distances in (c).

More recent attempts have been made in investigating residual dipolar couplings between quadrupolar nuclei [81], studying the cross-terms between quadrupolar and other interactions [82], elucidating relative orientations among quadrupolar nuclei [83] all of which are ultimately expected to yield more structural information.

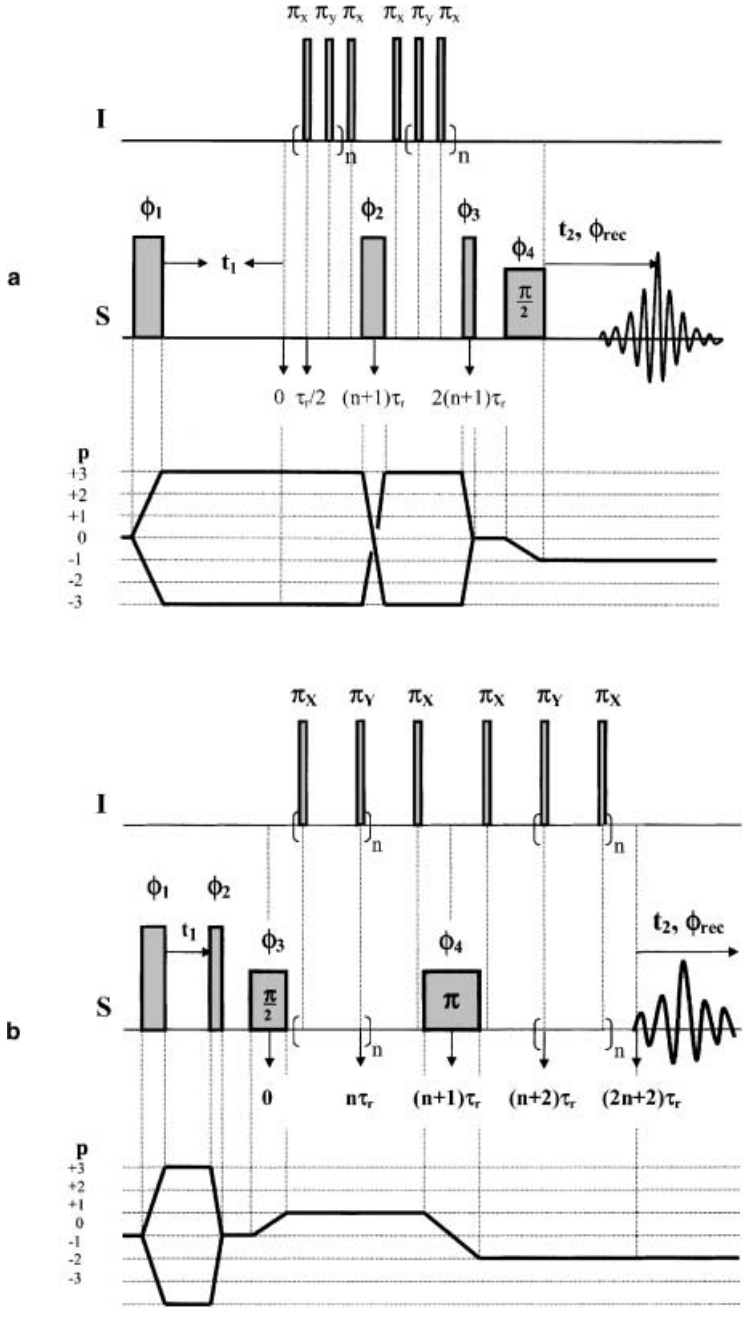

Fig. 15 (*continued*)

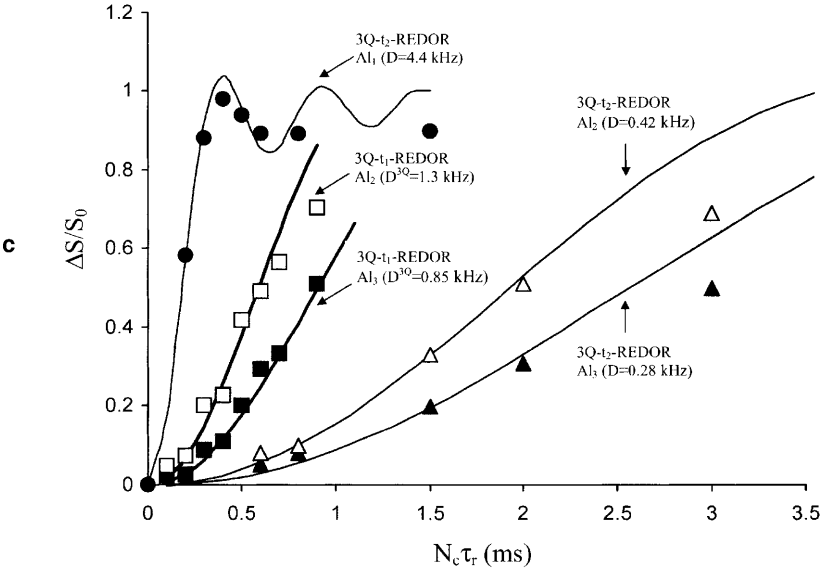

Fig. 15. (a) Pulse sequence used for 3Q-t_1-REDOR experiment. The phase cycle employed is as follows:

$\phi_1 = (0°)_{144}$,
$\phi_2 = (0°, 30°, 60°, \ldots, 330°)_{12}$,
$\phi_3 = [(0°)_{12}, (60°)_{12}, \ldots, (300°)_{12}]$,
$\phi_4 = (0°)_{72}, (180°)_{72}$,
$\phi_{rec} = [(0°, 180°)_6, (180°, 0°)_6]_3, [(180°, 0°)_6, (0°, 180°)_6]_3$.

A hypercomplex data set was collected by acquiring a complementary set of 96 fid's with $\phi_1 = 30°$. t_1 increments were rotor-synchronised.

(b) Pulse sequence used for 3Q-t_2-REDOR experiment. The phase cycle employed is as follows:

$\phi_1 = (0°)_{96}$,
$\phi_2 = (0°, 60°, 120°, 180°, 240°, 300°)_{16}$,
$\phi_3 = (0°)_{24}, (90°)_{24}, (180°)_{24}, (270°)_{24}$,
$\phi_4 = [(0°)_6, (90°)_6, (180°)_6, (270°)_6]_4$,
$\phi_{rec} = [(0°, 180°)_3, (180°, 0°)_3]_2, [(270°, 90°)_3, (90°, 270°)_3]_2, [(180°, 0°)_3, (0°, 180°)_3]_2, [(90°, 270°)_3, (270°, 0°)_3]_2$.

A hypercomplex data set was collected by acquiring a complementary set of 96 fid's with $\phi_1 = 30°$; t_1 increments were rotor-synchronised.

(c) Experimentally measured and simulated REDOR curves are shown for Al_1, Al_2 and Al_3 sites in $AlPO_4$-CHA obtained from 3Q-t_1-REDOR and 3Q-t_2-REDOR schemes. Analysis of the curves yielded the following distances: $r_{Al_3-F} = 4.1(\pm 0.1)$ and $r_{Al_2-F} = 4.7(\pm 0.1)$Å. (Reproduced with permission from Ref. [79], Coypright (1998), American Chemical Society and [80])

Common Applications

MQMAS has made study of various quadrupolar systems feasible in a routine way. Here, we outline a few representative examples of such investigations along with the type of information that may be extracted from MQMAS, possibly in conjunction with other experiments as well. The applications and observations are selected in a random order. The range of such studies is expected to increase with the advent of higher magnetic fields and by the use of sensitivity enhanced MQMAS schemes.

High Resolution ^{17}O NMR of Organic Solids

An important role for MQMAS is envisaged in the study of ^{17}O 3QMAS and 5QMAS experiments. This particular nucleus is expected to play a role in biomolecular structure determination with its high chemical shift dispersion. *Wu* [84] was the first to demonstrate the feasibility of such an experiment on some organic substances, [$^{17}O_2$]-D-alanine, potassium hydrogen [$^{17}O_4$] dibenzoate, [$^{17}O_4$]-D,L-glutamic acid-HCl and [2, 4-$^{17}O_2$] uracil. The 3QMAS spectrum of the glutamic acid is shown in Fig. 16. It is noted that substantial resolution can be achieved in these compounds with labelling of about 15–50% and moderate magnetic field of 11.75 T. Rotor synchronised t_1 increments were found to improve the signal-to-noise ratio. Besides providing information regarding isotropic chemical shift and quadrupolar parameters, ^{17}O MQ-MAS spectra are expected to shed light on several aspects of organic and biological systems, such as, H-bonding, side chain conformation, and base pairing in nucleic acids. One of the challenges in this field

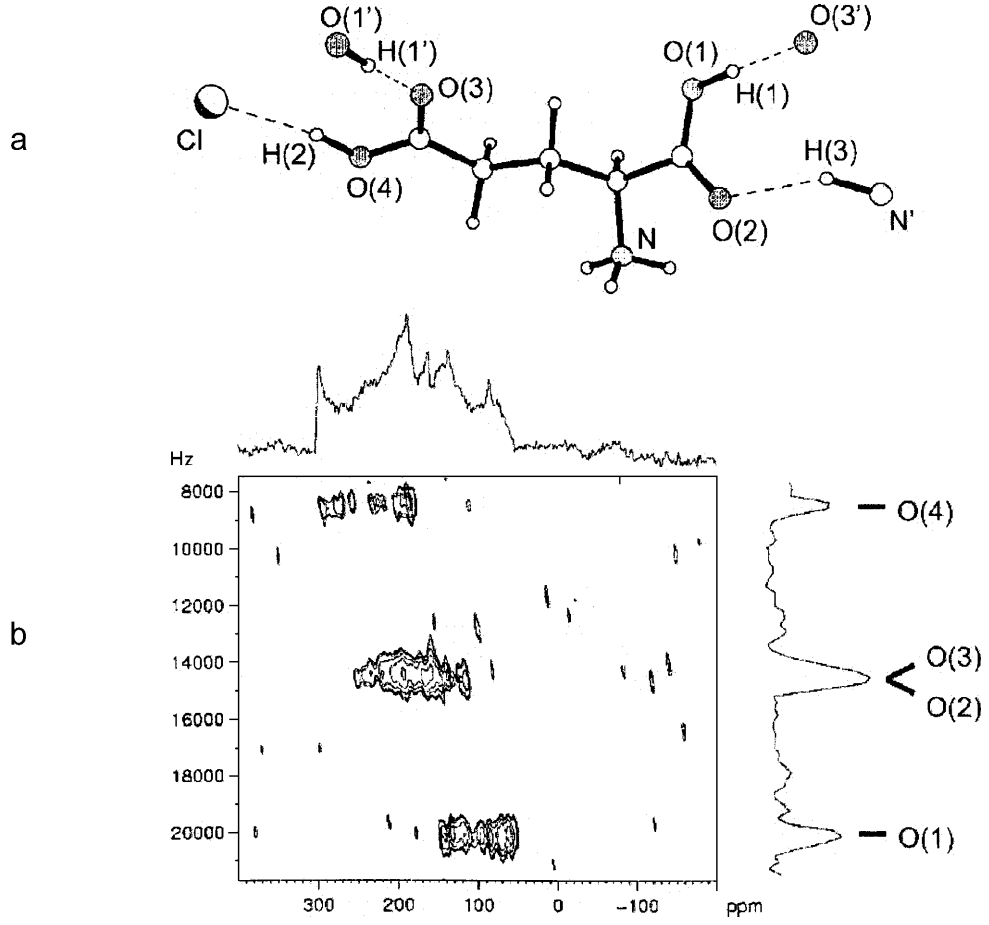

Fig. 16. (a) Molecular strucuture and ^{17}O positions marked of L-glutamic acid · HCL (b) ^{17}O 3QMAS spectrum of (a) with 28 rotor-synchronised t_1 increments. (Reproduced with permission from Ref. [84], Copyringht (2001), American Chemical Society)

lies in the synthesis of ^{17}O-enriched biological molecules together with the need to develop better sensitivity enhanced MQMAS schemes.

^{27}Al MQMAS: Study of Porous Materials

Zeolites play a big role in catalytic applications due to their stability and activity combined with a high selectivity. They are basically a unique class of porous solid aluminosilicates. ^{27}Al MAS NMR has been used in the past for a detailed study of aluminium coordination in zeolites [23, 85, 86]. However, the resulting spectra provide information that is normally restricted to aluminum coordination. Thus, resolving sites with similar environments is rarely achieved experimentally. ^{27}Al MQMAS, however, provides good resolution for the various ^{27}Al sites thereby allowing a near complete characterisation of such materials. When these materials are amorphous, details about the type of distribution become available. Properties like site specific dealumination [87] and positions and properties of acidic sites

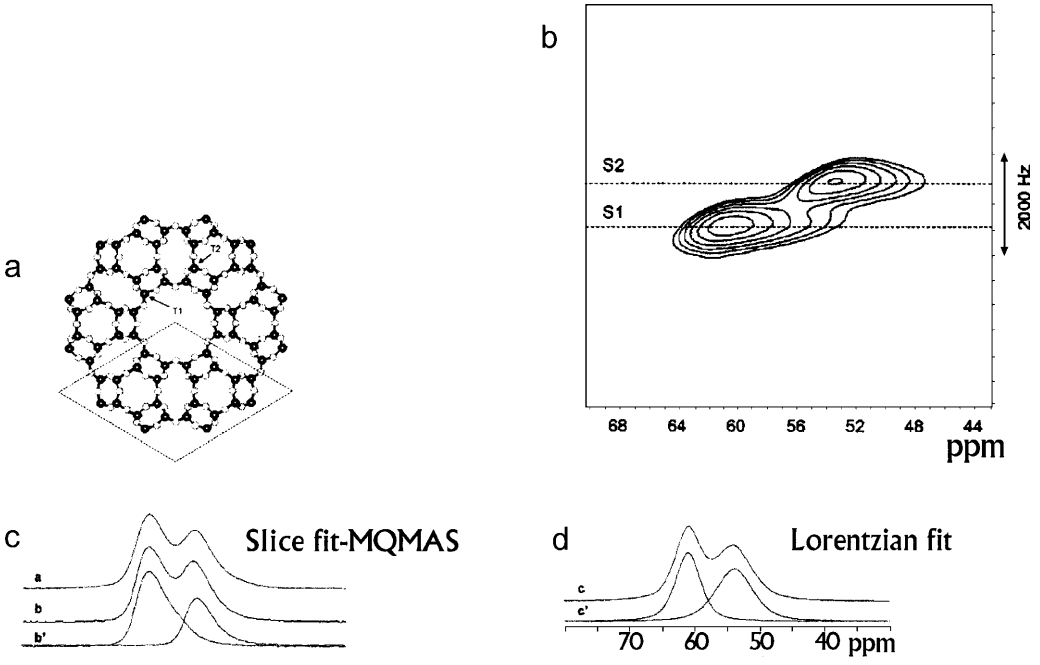

Fig. 17. (a) Projection of the MAZ zeolite along the *c*-axis, black circles are T atoms and light circles are the oxygen atoms. Tetrahedral framework aluminium sites are assigned to the Al atoms incorporated in the T1 and T2 crystallographic sites. (b) ^{27}Al 3QMAS spectrum of the MAZ zeolite sample with the horizontal axis corresponding to the F_2 dimension and the vertical axis corresponding to the F_1 dimension. The anisotropic slices corresponding to S1 and S2 are shown in (c) in the first row. Note the deviation of these lineshape from Lorentzian (d, first row) as assumed in the earlier studies. Also shown in (c) are the 1D ^{27}Al MAS spectrum of the MAZ zeolite (third row) and fitted spectrum (second row) using the slices S1 and S2 obtained from the 3QMAS spectrum. Also shown in (d) are the fitted spectrum (second row) using two Lorentzian shaped lines shown in the first row. A better fit may be found in (c) by virtue of the availability of true lineshapes due to resolution enhancement enabled by MQMAS spectrum. (Reproduced with permission from Ref. [90], Copyright (1999), American Chemical Society)

[88, 89] can be obtained unambiguously. *Wouters et al.* [90] demonstrated how MQMAS can give improved information about site populations. ^{27}Al MAS NMR studies have been used to arrive at the ratio of $\frac{Al^{T1}}{Al^{T2}}$ (corresponding to the two crystallographic sites, T_1 and T_2, Fig. 17a) in the mazzite zeolite. Slices along the MAS dimension of a 3QMAS spectrum (Fig. 17b) were used to deconvolute the 1D MAS spectrum (Fig. 17c), instead of the traditional Lorentzian/Gaussian lineshapes (Fig. 17d). The site population was shown to be completely different than previous reports (1.75 instead of 0.86) with a much better fit. It may be noted that, in general, site population estimates can be misleading in NMR experiments since the lineshapes and the positions of the lines are field dependent.

^{11}B MQMAS and MAS of Glasses

^{11}B MAS and MQMAS have been applied to a study of $x\mathrm{Na_2S} + (1-x)\mathrm{B_2S_3}$ glasses and polycrystals [91]. With the enhanced resolution from the MQMAS spectra, it

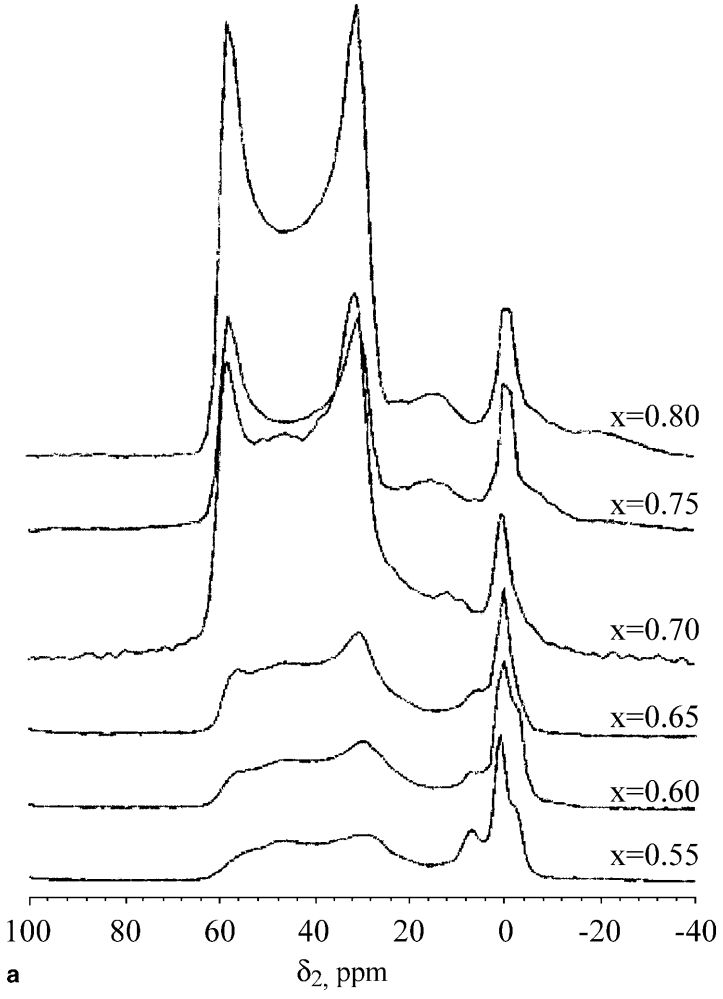

Fig. 18. (*continued*)

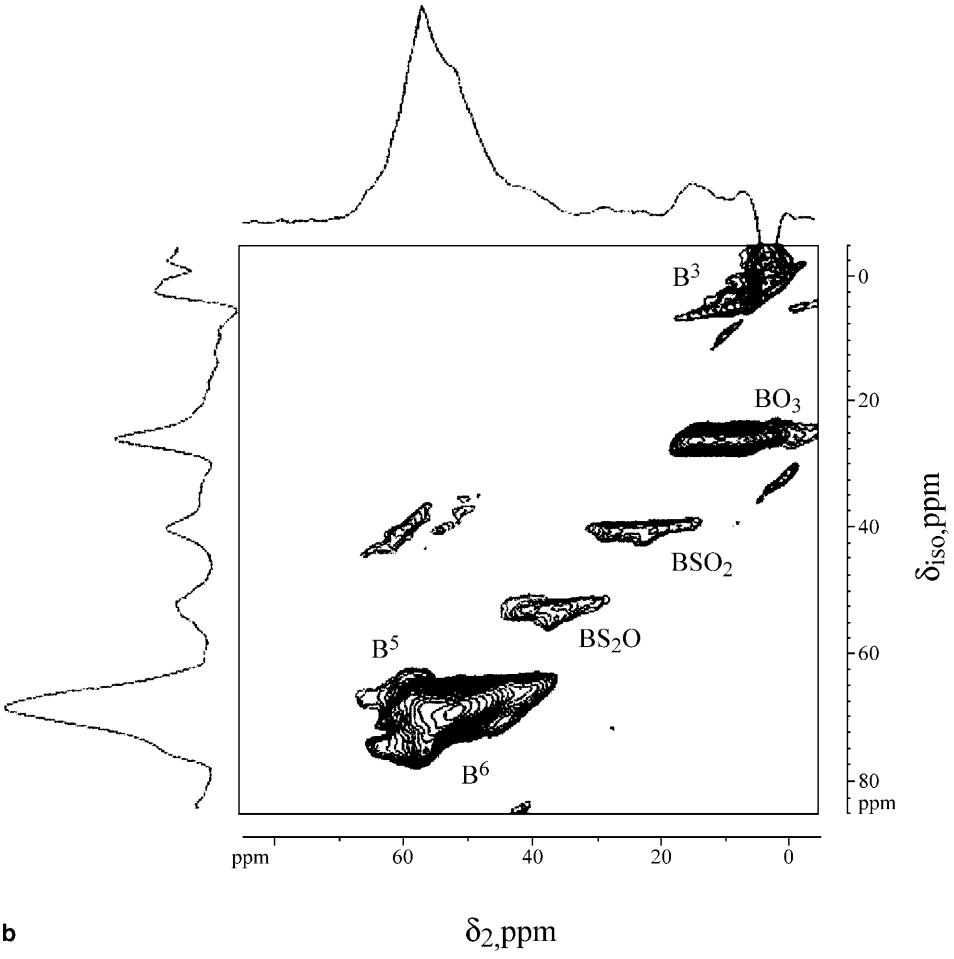

Fig. 18. (a) ^{11}B MAS NMR spectra at a magnetic field of 5.9 T of $xNa_2S + (1-x)B_2S_3$ glasses in the high alkali glass forming range $0.55 \leq x \leq 0.80$. (b) ^{11}B 3QMAS NMR spectrum taken at 9.4 T for the glass formed at $x = 0.6$. (Reproduced with permission from Ref. [91], Copyright (1998), American Chemical Society)

was possible to simulate corresponding MAS spectra and deduce isotropic chemical shift, quadrupolar parameters and relative concentrations of the various boron sites. Based on the known structure of boron trisulphide ($x = 0$), sodium methathioborate ($x = 0.5$) and sodium orthothioborate ($x = 0.75$), a model was suggested for the structure of sodium dithioborate ($x = 0.33$). In glasses, several structural units of the polycrystalline sample were observed alongside other new species. The evolution of the glass with an increasing Na_2B was tracked down and oxygen impurities were observed by MQMAS and MAS spectra with varying x values. The ^{23}Na spectra were not so informative due to the high mobility of the Na^+ ions, producing broad NMR spectra. Figure 18 shows the evolution of the MAS spectra of a glass formation with x between 0.55 and 0.8 (Fig. 18a) and a MQMAS spectrum of a glass formed at $x = 0.6$ (Fig. 18b). The evolution towards an orthothioborate ($x > 0.75$, large powder pattern at 40–60 ppm) is clearly observed. The oxygen impurities are detected in the MQMAS spectra in addition to other basic structural units.

Additional studies have been performed on aluminosilicates utilising ^{17}O and ^{27}Al MQMAS NMR [93, 92] providing information about bond angle distributions and coordinations.

Observation of Indirect Spin–Spin Couplings in Quadrupolar Nuclei

The indirect spin–spin coupling constant, J, which is a useful parameter providing insight into molecular structure and chemical bonding, is difficult if not impossible to measure in solid state NMR of quadrupolar systems. The splitting arising from J will be masked in the second-order quadrupolar broadening. The advent of MQMAS has made the observation of J possible as demonstrated by *Wu et al.* [94] in the ^{11}B $\left(I = \frac{3}{2}\right)$ 3QMAS spectrum of a solid borane–triphenylphosphite complex, (PHO_3P–BH_3). Two isotropic peaks representing a doublet pattern were found. The experiments were performed at two magnetic fields to confirm that the splitting was indeed from one-bond J coupling between ^{11}B and ^{31}P. The experimental spectrum and derived NMR parameters are shown in Fig. 19. The apparent splitting in the indirect dimension of MQMAS spectrum is 2.125 J thus leading to an enhanced resolution. This enhancement is generally higher for the highest order of MQC. For lower MQC in higher spin systems one gets a reduction in the J splitting (except for 7QC in spin-$\frac{9}{2}$) [94].

Co-ordination Environments of ^{25}Mg in Nucleic Acids

Magnesium, ^{25}Mg, is a spin-$\frac{5}{2}$ nucleus with a low NMR sensitivity. MQMAS has been shown to be effective for the resolution and assignment of Mg binding sites

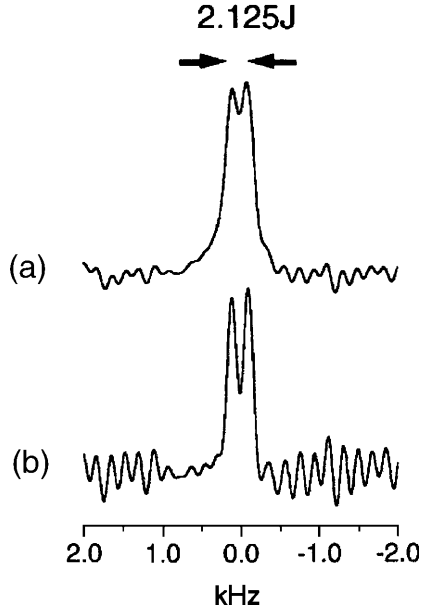

Fig. 19. ^{11}B 3QMAS spectra of $(PhO)_3P$–BH_3 at 7.4 T showing a J split doublet (a) with and (b) without resolution enhancement. The J splitting arises due to a $^1J(^{11}B, ^{31}P) = 85 \pm 5$ Hz as measured from the MQMAS spectrum. An analysis of the ^{11}B MQMAS spectra also yielded the following parameters: $\nu_Q = 1.22 \pm 0.02$ MHz, $\eta = 0.10 \pm 0.05$, and $\delta_{iso} = 3.0 \pm 0.1$ ppm. (Reproduced with permission from Ref. [94], Copyright (1994), American Chemical Society)

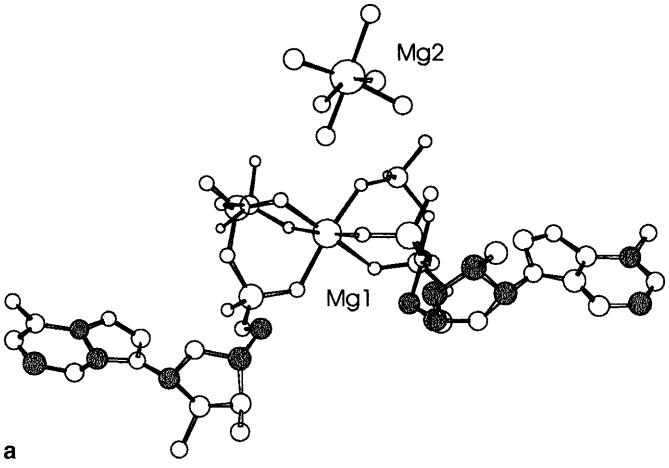

a

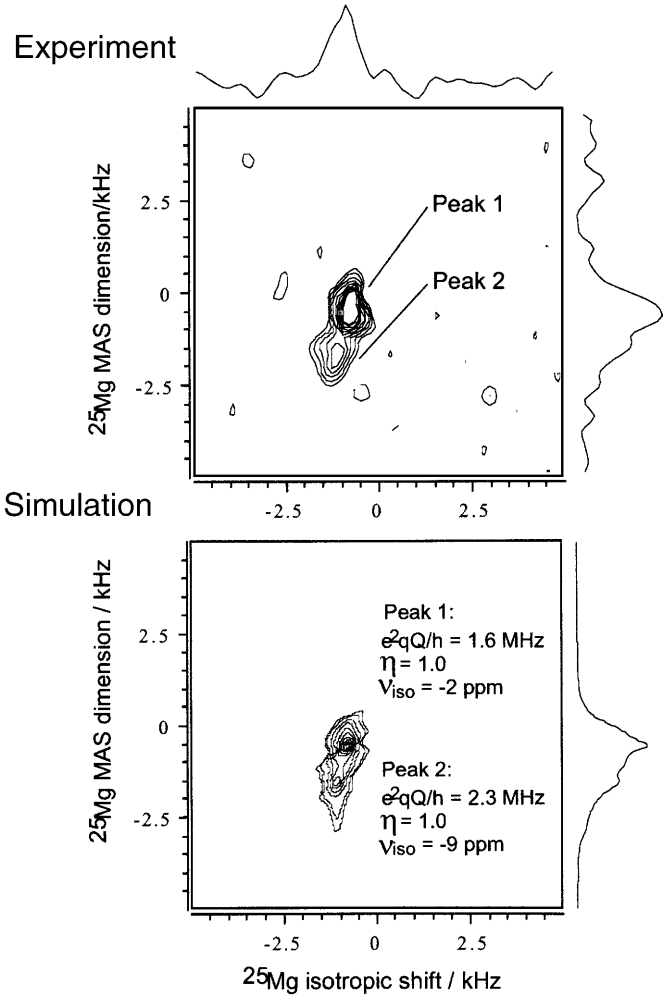

b

Fig. 20 (*continued*)

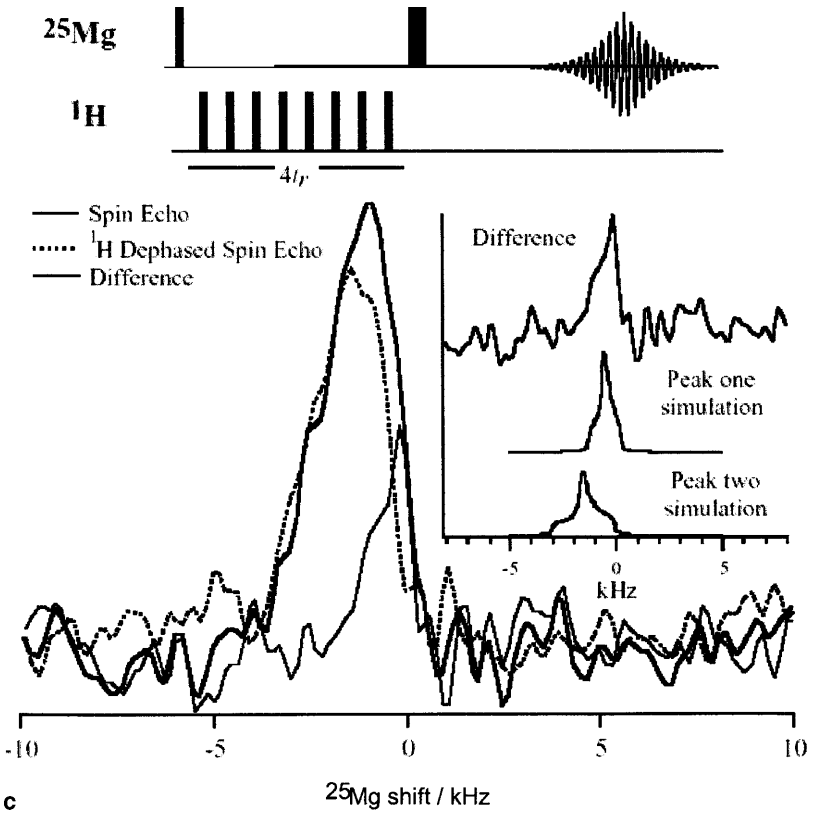

Fig. 20. (a) Illustration of the two magnesium coordination environments in MgATP/BPA. (b) Top spectrum is a ^{25}Mg 3QMAS spectrum of MgATP/BPA acquired with the following parameters, external magnetic field 11.7 T, $\nu_r = 10.0$ kHz, CW–CW pulse scheme with an excitation pulse of 7.5 μs and conversion pulse of 4.0 μs, number of transients of 24000 and number of t_1 increments of 16. Two magnesium peaks can be observed in the spectrum. The bottom spectrum is the best fit simulations of the experimental spectrum. The deduced parameters are indicated in the figure. (c) REDOR kind of pulse sequence and resulting difference curves that lead to the identification of which of the ^{25}Mg signal is being generated by each coordination environment shown in (a). The ^{25}Mg spin-echo data is obtained by the pulse sequence having $\frac{\pi}{2}$ and π pulses of duration 4.4 μs and 8.89 μs. An interpulse spacing of 400 μs had 8 ^{1}H π pulses inserted, centered at $\frac{1}{4}$ and $\frac{3}{4}$ of the rotor period. The inset graph compares the difference spectrum with the linseshapes simulated for peaks 1 and 2 using the parameters determined by MQMAS given in (b). (Reproduced with permission from Ref. [95], Copyright (2001), American Chemical Society)

within nucleic acids [95]. Figure 20a shows a ^{25}Mg 3QMAS spectrum of a ternary complex of magnesium(II), adenosine 5′-triphosphate, and bis(2-pyriyl)amine (BPA) ($[Mg(H_2O)_6][HBPA]_2[Mg(MATP)_2]$ $12H_2O$ (MgATP/BPA), a schematic of which is shown in Fig. 20b. The two crystallographically inequivalent Mg sites were resolved in the spectrum, and the NMR parameters were derived. A combination of this data with a 1D proton REDOR dephasing experiment, Fig. 20c, enabled an assignment of the two Mg peaks. Peak 1 corresponds to Mg(2) co-ordinated by water molecules, and thus dominates the REDOR difference spectrum. The weakly coupled peak 2 corresponds to Mg(1) which is co-coordinated entirely by phosphate oxygen donors. The experiment mentioned above highlights the potential of

^{25}Mg NMR as a tool for elucidating magnesium coordination environments in biological complexes.

Conclusions

In this review an outline of the MQMAS experiment together with the basic theory for MAS and MQMAS of half-integer quadrupolar nuclei was given. Several experimental protocols were explored together with a detailed description of possible sensitivity enhancement schemes. For a spin-$\frac{3}{2}$, FAM-RIACT-FAM proved to be a very efficient enhancement scheme giving rise to relatively undistorted lineshapes. FASTER-MQMAS can be used when only low rf power is available (20–70 kHz), however, lineshapes are severely distorted. DFS pulses perform at least as well as FAM and give the user an additional free parameter (frequency modulation) to play with. DFS pulses can also be applied to low-γ nuclei with spin-$\frac{5}{2}$, since only low rf power levels are needed. When hardware is not suitable for these pulses, spin-$\frac{5}{2}$ MQMAS can be obtained with the aid of FAM-II pulses. The data analysis procedure was discussed in detail thus giving an accurate way to extract the relevant NMR parameters, *i.e.* NQCC and chemical shift. Heteronuclear experiments with high-resolution detection of the quadrupolar nucleus were explored and finally, some representative applications of the MQMAS experimental method were demonstrated.

Acknowledgements

The authors thank Prof. *S. Vega* for many discussions and suggestions on the manuscript. Discussions with Prof. *L. Frydman* are gratefully acknowledged. We thank Dr. *T. Bräuniger* and *M. Carravetta* for a critical reading of the manuscript. We thank Dr. *A. J. Vega* for providing us with the data which was used for the generation of Fig. 3.

References

[1] Abragam A (1961) The Principles of Nuclear Magnetism. Clarendon Press, Oxford
[2] Duer M (2002) Solid-State NMR Spectroscopy: Principles and Applications. Blackwell Science
[3] Pound RV (1950) Phys Rev **79**: 685
[4] Andrew ER, Bradbury A, Eades RG (1958) Nature **182**: 1659
[5] Lowe IJ (1959) Phys Rev Lett **2**: 285
[6] Vega AJ (1992) J Magn Reson **78**: 245
[7] Vega AJ (1992) Solid State NMR **1**: 17
[8] Samoson A, Lippmaa E, Pines A (1988) Mol Phys **65**: 1013
[9] Llor A, Virlet J (1988) Chem Phys Lett **152**: 248
[10] Chmelka BF, Müller KT, Pines A, Stebbins J, Wu Y, Zwanziger JW (1989) Nature **339**: 42
[11] Frydman L, Harwood JS (1995) J Am Chem Soc **117**: 5367
[12] Medek A, Harwood JS, Frydman L (1995) J Am Chem Soc **117**: 12779
[13] Gan Z (2000) J Am Chem Soc **122**: 3242
[14] Wu Y (1996) Encyclopedia of Nuclear Magnetic Resonance, Wiley, 1749
[15] Grandinetti PJ (1996) Encyclopedia of Nuclear Magnetic Resonance. Wiley, p 1768
[16] Gan Z (2001) J Chem Phys **114**: 10845
[17] Vega AJ (1996) Encyclopedia of Nuclear Magnetic Resonance. Wiley, p 3869

[18] Cohen MH, Reif F (1957) Solid State Phys 5. Academic Press Inc, p 321
[19] Rose ME (1957) Elementary Theory of Angular Momentum. Wiley, New York
[20] Zheng ZW, Gan Z, Sethi NK, Alderman DW, Grant DM (1991) J Magn Reson **95**: 509
[21] Man PP (1996) Encyclopedia of Nuclear Magnetic Resonance. Wiley
[22] Lippmaa E, Samoson A, Mägi M (1986) J Am Chem Soc **108**: 1730
[23] Kentgens APM (1997) Geoderma **80**: 271
[24] Vega S, Naor Y (1981) J Chem Phys **75**: 75
[25] Gerstein BC (1996) Encyclopedia of Nuclear Magnetic Resonance. Wiley, p 3360
[26] Ganapathy S, Schramm S, Oldfield E (1982) J Chem Phys **77**: 4360
[27] Jakobsen HJ, Skibsted J, Bildsøe H, Nielsen NC (1989) J Magn Reson **85**: 173
[28] Gan Z (2001) J Chem Phys **114**: 10845
[29] Dirken PJ, Kohn SC, Smith ME, van Eck ERH (1997) Chem Phys Lett **266**: 568
[30] Hwang SJ, Fernandez C, Amoureux JP, Han JCJW, Martin SW, Pruski M (1998) J Am Chem Soc **120**: 7337
[31] Fyfe CA, zu Altenschildesche HM, Skibsted J (1999) Inorg Chem **38**: 84
[32] Ferreira A, Lin Z, Rocha J, Morais CM, Lopes M, Fernandez C (2001) Inorg Chem **40**: 3330
[33] Lefebvre F, Amoureux JP, Fernandez C, Deronane EG (1987) J Chem Phys **86**: 6070
[34] Jerschow A, Logan JW, Pines A (2001) J Magn Reson **149**: 268
[35] Pike KJ, Malde RP, Ashbrook SE, McManus J, Wimperis S (2000) Solid State NMR **16**: 203
[36] Ernst R, Bodenhausen G, Wokaun A (1988) Principle of NMR in One and Two Dimensions. Oxford
[37] Bodenhausen G (1981) Prog Nucl Magn Reson Spectrosc **14**: 137
[38] Vega S, Pines A (1977) J Chem Phys **66**: 5624
[39] Wu G, Rovnyak D, Sun BQ, Griffin RG (1996) Chem Phys Lett **249**: 210
[40] Massiot D, Touzo B, Trumeau D, Coutures JP, Virlet J, Florian P, Grandinetti PJ (1996) Solid State NMR **6**: 73
[41] Schmidt-Rohr K, Spiess HW (1996) Multidimensional Solid State NMR and Polymers. Academic Press, pp 155–156
[42] Amoureux JP, Fernandez C, Steuernagel S (1996) J Magn Reson **A123**: 116
[43] Bax A, Mehlkopf AF, Smidt J (1979) J Magn Reson **35**: 373
[44] Brown SP, Heyes SJ, Wimperis S (1996) J Magn Reson **A119**: 280
[45] Brown SP, Wimperis W (1999) J Magn Reson **124**: 279
[46] Man PP (1998) Phys Rev B **58**: 2764
[47] Millot Y, Man PP (2002) Solid State NMR **21**: 21
[48] Goldbourt A, Vega S (2002) J Magn Reson **154**: 280
[49] Herreros B, Metz AW, Harbison GS (2000) Solid State NMR **16**: 141
[50] Engelhardt G, Koller H (1991) Magn Reson Chem **29**: 941
[51] Amoureux JP, Pruski M, Lang DP, Fernandez C (1998) J Magn Reson **131**: 17
[52] Massiot D (1996) J Magn Reson **A122**: 240
[53] Larsen FH, Skibsted J, Jakobsen HJ, Nielsen CN (2000) J Am Chem Soc **122**: 7080
[54] Marinelli L, Medek A, Frydman L (1998) J Magn Reson **132**: 88
[55] Wu G, Rovnyak D, Griffin RG (1996) J Am Chem Soc **118**: 9326
[56] Lim KH, Grey CP (1998) Solid State NMR **13**: 101
[57] Caldarelli S, Ziarelli F (2000) J Am Chem Soc **122**: 12015
[58] Kentgens APM, Verhagen R (1999) Chem Phys Lett **300**: 435
[59] Madhu PK, Goldbourt A, Frydman L, Vega S (1999) Chem Phys Lett **307**: 41
[60] Madhu PK, Goldbourt A, Frydman L, Vega S (2000) J Chem Phys **112**: 2377
[61] Iuga D, Schäfer H, Verhagen R, Kentgens APM (2000) J Magn Reson **147**: 192
[62] Schäfer H, Iuga D, Verhagen R, Kentgens APM (2001) J Chem Phys **114**: 3073
[63] Goldbourt A, Madhu PK, Kababya S, Vega S (2000) Solid State NMR **18**: 1
[64] Yao Z, Kwak H-T, Sakellariou D, Emsley L, Grandinetti PJ (2000) Chem Phys Lett **327**: 85

[65] Kwak H-T, Prasad S, Yao Z, Grandinetti PJ, Sachleben JR, Emsley L (2001) J Magn Reson **95**: 509
[66] Madhu PK, Levitt MH (2002) J Magn Reson **155**: 150
[67] Vosegaard T, Florian P, Massiot D, Grandinetti PJ (2001) J Chem Phys **114**: 4618
[68] Vosegaard T, Massiot D, Grandinetti PJ (2000) Chem Phys Lett **326**: 454
[69] Goldbourt A, Madhu PK, Vega S (2000) Chem Phys Lett **320**: 448
[70] Pruski M, Lang DP, Fernandez C, Amoureux JP (1997) Solid State NMR **7**: 327
[71] Fernandez C, Develoye L, Amoureux JP, Lang DP, Pruski M (1997) J Am Chem Soc **119**: 6858
[72] Ashbrook SE, Wimperis S (2001) Chem Phys Lett **340**: 500
[73] Ashbrook SE, Brown SP, Wimperis S (1998) Chem Phys Lett **288**: 509
[74] Ashbrook SE, Wimperis S (2000) J Magn Reson **147**: 238
[75] Rovnyak D, Baldus M, Griffin RG (2000) J Magn Reson **142**: 145
[76] Wang SH, De Paul SM, Bull LM (1997) J Magn Reson **125**: 364
[77] Gullion T, Schaefer J (1989) J Magn Reson **81**: 196
[78] Gullion T (1995) Chem Phys Lett **246**: 325
[79] Fernandez C, Lang DP, Amoureux JP, Pruski M (1998) J Am Chem Soc **120**: 2672
[80] Pruski M, Baily A, Lang DP, Amoureux JP, Fernandez C (1999) Chem Phys Lett **307**: 35
[81] Wi S, Frydman L (2000) J Chem Phys **112**: 3248
[82] McManus J, Kemp-Harper R, Wimperis S (1999) Chem Phys Lett **311**: 292
[83] Dowell NG, Ashbrook SE, McManus J, Wimperis S (2001) J Am Chem Soc **123**: 8135
[84] Wu G, Dong S (2001) J Am Chem Soc **123**: 9119
[85] Alemany ML (1993) Appl Magn Reson **4**: 179
[86] Smith ME (1993) Appl Magn Reson **4**: 1
[87] van Bokhoven JA, Koningsberger DC, Kunkeler P, van Bekkum H, Kentgens APM (2000) J Am Chem Soc **122**: 12842
[88] Kentgens APM, Iuga D, Kalwei M, Koller H (2001) J Am Chem Soc **123**: 2925
[89] Blumenfeld AL, Fripiat JJ (1997) J Phys Chem **101**: 6670
[90] Wouters BH, Chen T, Goossens AM, Martens JA, Grobet PJ (1999) J Phys Chem **B103**: 8093
[91] Hwang SJ, Fernandez C, Amoureux JP, Han JW, Cho J, Martin SW, Pruski M (1998) J Am Chem Soc **12**: 7337
[92] Baltisberger JH, Xu Z, Stebbins JF, Wang SH, Pines A (1996) J Am Chem Soc **118**: 7209
[93] Lee SK, Stebbins JF (2000) J Phys Chem **B104**: 4091
[94] Wu G, Kroeker S, Wasylishen RE, Griffin RG (1997) J Magn Reson **124**: 237
[95] Grant CV, Frydman V, Frydman L (2000) J Am Chem Soc **122**: 11743
[96] Hoult DI, Richards RE (1975) Proc Royal Soc (London) **A344**: 311
[97] Stejskal EO, Schaefer J (1975) J Magn Reson **18**: 560